Science Journal of Chemistry
2023; 11(5): 168-188
http://www.sciencepublishinggroup.com/j/sjc
doi: 10.11648/j.sjc.20231105.11
ISSN: 2330-0981 (Print); ISSN: 2330-099X (Online)

Schiff Base and Its Metal Complexes as Ecofriendly Pitting Corrosion Inhibitors on ASTM-$_{A3}$6 Low Carbon Steel in Corrosive Oil and Gas Well Treatment Fluids

Chimezie Peter Ozoemena[1, *], Ekerete Jackson Boekom[1], Ekaete Jacob Abai[2], Essien Kufre Edet[3], Inemesit Asuquo Akpan[1]

[1]Department of Chemistry, University of Uyo, Uyo, Nigeria

[2]Akwa Ibom State Polytechnic, Ikot Ekpene, Nigeria

[3]Department of Chemistry, Akwa Ibom State University, Ikot Akpaden, Nigeria

Email address:

chimexpet47@yahoo.com (Chimezie Peter Ozoemena), ekereteboekom@gmail.com (Ekerete Jackson Boekom)

[*]Corresponding author

To cite this article:

Chimezie Peter Ozoemena, Ekerete Jackson Boekom, Ekaete Jacob Abai, Essien Kufre Edet, Inemesit Asuquo Akpan. Schiff Base and Its Metal Complexes as Ecofriendly Pitting Corrosion Inhibitors on ASTM-A36 Low Carbon Steel in Corrosive Oil and Gas Well Treatment Fluids. *Science Journal of Chemistry*. Vol. 11, No. 5, 2023, pp. 168-188. doi: 10.11648/j.sjc.20231105.11

Received: June 16, 2023; **Accepted**: August 14, 2023; **Published**: September 15, 2023

Abstract: A high yield (74.63%) bidentate Schiff base ligand was synthesized from the condensation reaction of 4-aminophenol and 4-diethylamino-2-hydroxybenzaldehyde by the reflux method. Its transition metal complexes of Ni, Cu and Zn were prepared from the corresponding metal salts in methanol solution using the same procedure. The chemical structure of the synthesized Schiff base and its metal complexes was characterized by physicochemical, spectral analysis (FTIR and UV-Visible), and molar conductivity studies which revealed that the metal complexes were non electrolytic. Elemental analysis data for the Schiff base ligand and its metal complexes were used to confirm the general formula of the compound. The spectral data showed that coordination occurred through the azomethine nitrogen atom and the oxygen atom of the phenolic ring. The corrosion inhibition of Schiff base and its metal complexes was evaluated using potentiodynamic polarization (PDP), linear polarization resistance (LPR), and weight loss (WL) methods in acidic oil and gas well treatment fluid. The corrosive fluid was simulated using 1 M HCl solution. The results indicated that the compounds had a promising inhibitory effect on the corrosion of ASTM-A36 low carbon steel in the medium. The effectiveness of the inhibitors decreased with increasing time and temperature, but improved with increasing concentration of the inhibitors. The metal complexes showed a synergistic effect against Schiff base, with NiL1 having the maximum inhibition efficiency of 84.29%. The thermodynamic parameters revealed that the adsorption of the Schiff base and its complexes on the metal surface was spontaneous, endothermic and followed physical adsorption mechanism which conformed perfectly to the Langmuir adsorption isotherm. PDP measurements showed that the Schiff base and its metal complexes acted as mixed type inhibitors. The inhibition efficiency values obtained from the different techniques were comparable. SEM analyses of the corrosion product also confirmed the formation of a protective layer on the metal surface.

Keywords: Corrosion Inhibition, Schiff Base Ligand, Synthesis, Characterisation

1. Introduction

The role of corrosion chemistry in oil and gas industry cannot be overstated owing to its devastating effects on depletion of existing wells and petting of material [1-2]. Corrosion can be defined as the spontaneous deterioration of materials, especially metals, when exposed to a corrosive environment. Metal degradation already encompasses a large number of damages originating from inside the metal application area and outside the metal-based environment. The nature and composition of metals change due to corrosion caused by processes such as pH, temperature, oxide formation and hydrogen embrittlement. This is due to the

reduction in strength, appearance, permeability to liquids and gases, and the life span of the metal due to the presence of certain gases such as CO_2 and H_2S. Corrosion is a continual process and cannot completely be eliminated [3-6].

Corrosion is very costly and has a major impact on the social and economic conditions in industrialized countries. The annual cost of corrosion includes both direct and indirect costs that have a real impact on the gross domestic product (GDP) of many countries, which spent billions of dollar in putting up their industries. Therefore, corrosion cost is not only calculated in terms of economic losses, but also system failures during various incidents such as oil spills in truck pipelines, canned food spills, traffic accidents caused by wear of bolts and nuts, environmental pollution, replacement of materials, and loss of lives and properties [3, 7-10]. Corrosion can be electrochemical/wet or dry, depending on the interacting media [11]. Pitting corrosion is a form of localized corrosion that involves the formation of cavities and pores in a material [12-14]. For flawless materials, pitting corrosion can be caused by the environment, which can contain harsh chemicals that destroy the passive (oxide) film, thereby initiating pitting corrosion at oxide fractures (Figure 1) [15-17].

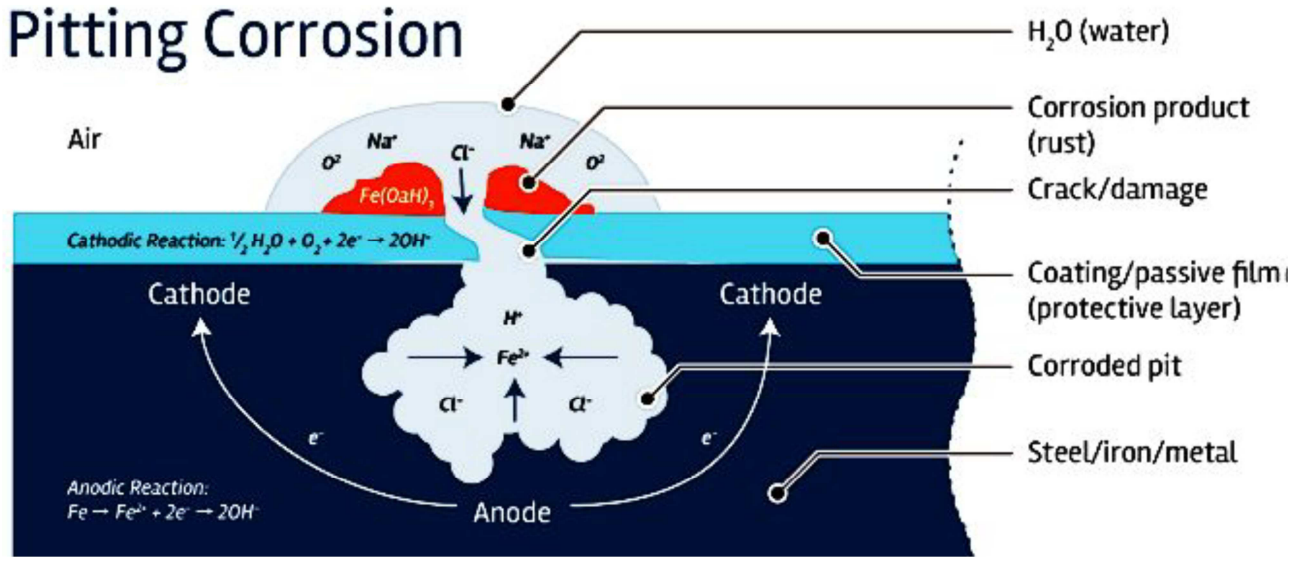

Figure 1. *A Typical Pitting Corrosion Process.*

Conversely, production can be increased through the use of certain chemicals in well stimulation, reservoir flooding, acid fracturing, and secondary and enhanced oil recovery operations. Stimulation or acidification is the most important field of application for the procedures that bring aggressive fluids into contact with structural steel materials [2]. During this process, acid is forced through the well under high pressure by the drill bit to chemically react with rocks (dolomite, calcite and limestone) that form the reservoir rock formations, dissolve them to open new flow channels, and enlarge existing ones [18]. Other areas related to well acidification procedures include scaling, drilling mud damage, hydraulic fracturing and matrix acidification techniques [19, 20]. During rupturing, fractures are produced in the formation and an acid solution is introduced into the fractures to line the flow channel and expand the pore space [20]. Compared to other acids (Formic, acetic and hydrofluoric, sometimes mixed with other concentrated acids), hydrochloric acid is the most commonly used in acidification because it is more economical and reacts very quickly with formations, but it is very corrosive. Therefore, the acid must be mixed with a corrosion inhibitor to protect the steel surfaces it comes in contact with from corrosion and pitting [21].

Corrosion inhibitors are an important class of oilfield chemicals which are essential as additives for acidic oil recovery fluids. Inhibitors are substances that reduce corrosion attack by modifying the environment. Therefore, adding small amounts of these chemicals to the paint stripper can reduce corrosion of exposed metals [22, 23]. This preventive measure is known as corrosion inhibition. Inhibitors reduce the anodic dissolution rate of the metal or cathodic reduction rate of the conjugate reaction which promotes corrosion process. So with this concept, there can be anodic, cathodic and mixed inhibitors. Inhibitors can be organic or inorganic, green or toxic [24].

The search for environmentally friendly inhibitors has led to cutting edge research using synthetic Schiff bases for corrosion resistance in almost all media, especially acidic media [25]. The increasing popularity of Schiff bases in corrosion science has been attributed to their low raw material cost, relatively easy synthetic routes, high purity, low toxicity and eco-friendly properties. Schiff bases, named after a German chemist Hugo Schiff (1864), are formed by the condensation of primary amines (1) with an aldehyde or ketone (2). Structurally, a Schiff base (3) molecule consists of benzene rings with delocalised π-electrons and electron rich substituents (–NO_2, –Cl, and –OH groups) (Figure 2). This structural feature facilitates better interaction with mild steel surfaces due to the presence of azomethine group (–

C=N–) in the molecule [26].

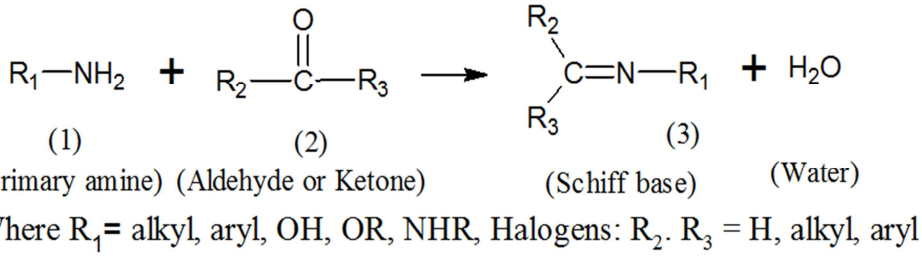

Figure 2. *General preparation method for Schiff base.*

Schiff base is a potential chelating ligand in coordination chemistry, and it has shown wide application prospects in medicine as anti-oxidants, antimicrobial agents and anti-inflammatory agents, as well as in industry as dye and pigment precursors, and corrosion inhibitors [27, 28]. Schiff bases are able to form coordinate bonds with many metal ions via imine nitrogens and other groups, usually linked to the aldehyde, they are mostly bidentate, tridentate or tetradentate ligands, capable to form very stable complexes with transition metals [26, 29]. The structural diversity and electronic properties of Schiff bases have led to the synthesis of a wide range of transition metal complexes, some of which have enhanced capabilities in corrosion science [25].

Moreover, different ligands of Co (II), Ni (II), Zn (II) and Sn (II) metal complexes showed good corrosion inhibition performance in different acidic media at room temperature and elevated temperatures, [30, 31]. Transition metal complexes derived from Schiff' bases are more effective inhibitors due to their larger size and compactness, and metal-organic hybrids are also synergistic [32]. Hence, in this research work, the inhibitory properties of a Schiff base synthesized by reacting 4-aminophenol and 4-diethylamino-2-hydroxybenzaldehyde with their transition metal complexes in 1M HCl solution on carbon steel is reported.

2. Material and Method

2.1. Materials

All reagents used in this study were obtained from Sigma Aldrich, Germany; and were used without further purification. Melting points were determined using Galenkemp melting point apparatus. Elemental analyses (C, H, and N %) were recorded on a Perkin-Elmer model 2400 Series II CNHS/O analyzer. The molar conductivity measurement were carried out using Jenway conductivity meter 4010 Model at room temperature. Magnetic susceptibility measurements were performed using magnetic susceptibility balance model 29275 at room temperature. FT-IR spectra of the Schiff base ligands were recorded on a SHIMADZU FTIR-8400 spectrophotometer in the 400-4000cm^{-1} range using KBr matrix. Electronic spectra of the ligands in ethanol solution were scanned in the range 300 - 800 nm on a UV - 2500 PC spectrophotometer. The weight loss measurement were conducted using thermostated water bath, Mettler Toledo PB602 analytical weighing balance and glass wares. Electrochemical studies were performed in a conventional three electrodes cell using computer-controlled potentiostat/galvanostat (Autolab PGSTAT 302N). Different grades of silicon carbide papers in the range of 400 to 1200 were used for surface abrasion.

2.2. Methods

2.2.1. Preparation of Specimens

The ASTM-A36 low carbon steel used in this research was obtained from Emma and Sons Nigeria limited, Okigwe, Imo State, Nigeria. The elemental composition of the mild steel by weight percentage was C – 0.17, Si – 0.26, Mn – 0.46, P – 0.0047, S – 0.017, Fe – 98.935. The ASTM-A36 low carbon steel specimens were mechanically pressed cut into coupons of dimension 4 x 3 x 0.017 cm. The coupons were polished with series of emery paper of variable grades starting with the coarsest and then proceeding in steps to the finest grade. They were washed with distilled water, rinsed with absolute ethanol, dried in air after rinsing with acetone which was in accordance with NACE Recommended Practice for surface finishing and cleaning of weight-loss coupons. In addition, coupons for electrochemical studies were mechanically press cut into coupons of dimensions 10mm by 10mm. The specimens were embedded with connecting terminal in epoxy resin leaving a working area of 1 cm^2. The surface preparation of the mechanically abraded specimens was carried out using silicon carbide emery paper of different grades (400 to 1200 grit) and subsequent cleaning with acetone and rinsing with distilled water prior to electrochemical measurement in 1 M HCl solution which was prepared by diluting 83ml of 37% HCl (Merck) stock to 1L standard flask with distilled water as corrosive environment. Finely polished low carbon steel was exposed to1.0 M HCl in the presence and absence of inhibitors (SBL1, NiL1, CuL1 and ZnL1). The solutions of the Schiff base and its metal complexes having the concentration of 20, 40, 60, 80 and 100 ppm were prepared.

2.2.2. Synthesis of Schiff Base Ligand (SBL) and Its Metal (II) Complexes

The Schiff base ligand (SBL) was synthesized according to literature methods with few modifications [33]. 4-aminophenol (1.36g, 0.01mol) was added to a 30 mL magnetically stirred ethanolic solution of 4-diethylamino-2-

hydroxybenzaldehyde (1.74g, 0.01mol) in a 100 mL round bottom flask (Figure 3). 2.5 mL of glacial acetic acid were added to the mixture to adjust its pH and then refluxed for 6 h upon which a bronze precipitate was formed instantly on cooling. The resulting precipitate was filtered, recrystallized with ethanol and dried in vacuum oven at 80°C.

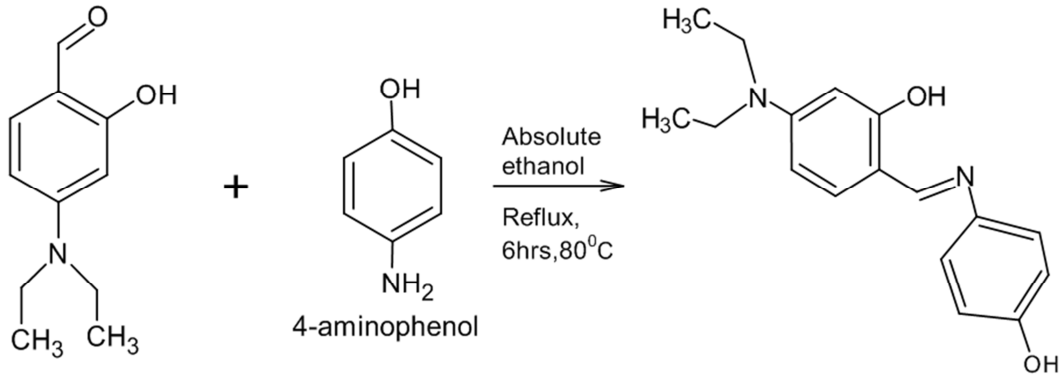

Figure 3. *Synthesis of the Schiff base ligand (1), SBL1, ($C_{17}H_{20}N_2O_2$).*

The metal complexes of the Schiff base ligand were prepared by mixing the synthesized Schiff base ligand (L1) (0.02mol) in 30 mL methanol with the corresponding metal salts (0.01mol) in a 100 mL round-bottomed flask. Few drops of glacial acetic acid were added and refluxed with constant stirring for 4 h at 40°C (Figure 4). On cooling colored complexes were precipitated and the resulting precipitates were then filtered, recrystallized with ethanol and dried in vacuum oven at 80°C.

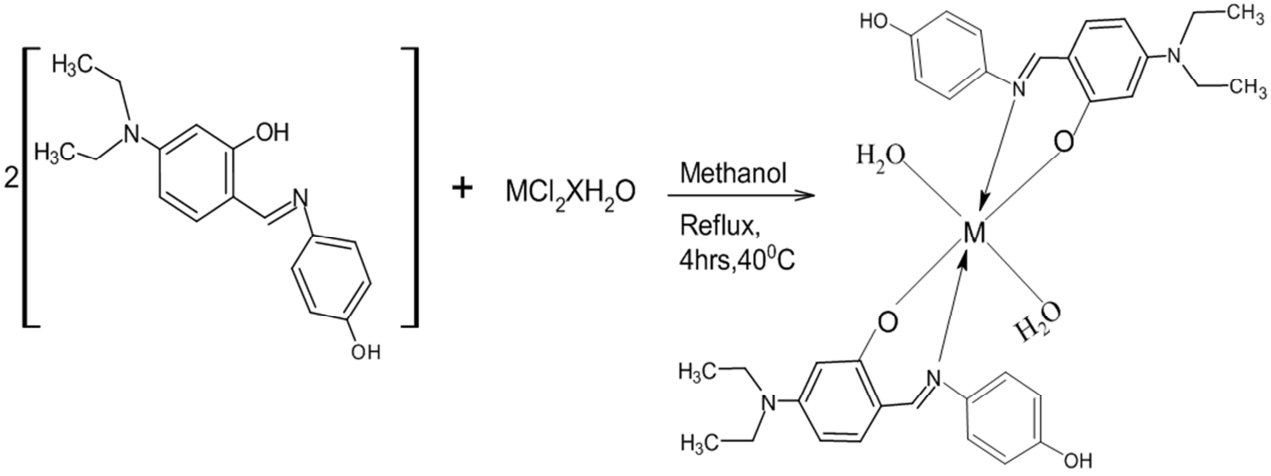

Where M= Zinc (II), Nickel (II) and Cupper (II), and X = 1, 2, 3 or 4

Figure 4. *Synthesis of Metal (II) Schiff Base Ligand (1) Complexes.*

2.2.3. Solubility Test and Melting Point Determination

The solubility test of the prepared Schiff base ligands and their metal complexes were determined in different solvents such as distilled water, ethanol, methanol, dimethylsulfoxide, dimethylformanide, acetone and acetic acid by shaking a small amount of each of the compounds in a test tube containing 10 mL portions of each of the solvents.

The melting point of the Schiff base, as well as the decomposition temperature of the metal complexes were determined by introducing a small amount of each samples into a capillary tube and then inserted into Gallenkamp melting point Apparatus, the temperature at which the ligands melted and the complexes decomposed were recorded.

2.2.4. Molar Conductivity and Magnetic Susceptibility Measurements

Molar conductance of the complexes were carried out in dimethylsulfoxide (DMSO) by dissolving 0.001M of each sample in 10mL of the solvent in a test-tube, the electrode were inserted and the reading were taken to determine the neutrality/electrolytic nature of the solvent. The molar conductance is given as:

$$\text{Molar conductance} = \frac{1000K}{Molar\ Concentration} \quad (1)$$

Where K is the specific conductance

The Magnetic Susceptibility of the metal complexes were also determine by introducing the prepared metal complexes into a capillary tube up to a given mark and the readings were

recorded using the magnetic susceptibility balance.

$$Xg = \frac{C_{bal} \times L(R-R_o)}{10^9 \times M} \quad (2)$$

$$X_m = Molar\ mass \times X_g \quad (3)$$

$$U_{eff} = 2.828\sqrt{X_m T} \quad (4)$$

Where C_{bal} is the constant of proportionality = 1, L = Sample length (cm), M = Sample mass

R = Reading for tube + sample, Ro = Empty tube reading, Xg = Mass Susceptibility, Xm = Molar Susceptibility.

2.2.5. Elemental Analysis

The elemental analysis (CHN) of the Schiff base and its metal complexes were conducted to find the appropriate molecular formula of the compounds and the results obtained using the micro-analytical instrument were compared with the calculated values.

2.2.6. Spectroscopic and Surface Characterization

The electronic absorption spectra also known as UV-Visible spectra are often very useful in structural elucidation. The electronic spectral measurements were used to assign the streochemistries of the metal ions in the complexes based on the positions and number of d-d transition peaks. Electronic spectra of the ligands were taken in absolute ethanol (10^{-3}). The IR spectra of the ligands and their metal complexes were carried out for structural elucidation and to determine the compounds responsible for adsorption to the metal surface. For weight loss measurements, the coupons were dipped in 150 mL of 1.0 M of HCl acid containing the studied Schiff base ligand and its metal complexes to form an adsorbed layer. The corrosion products were left for three days in 1.0 M HCl without and with 100ppm of the studied inhibitors, after which they were retrieved, dried, and the films scraped. The films were collected and subjected to IR analysis as reported elsewhere [34]. The samples were prepared using KBr and the analysis were done by scanning the sample through a wave number range of 400–4,000 cm−1 [34, 35].

2.2.7. Scanning Electron Microscope (SEM) Analysis

Morphological studies of the mild steel surfaces exposed to uninhibited and inhibited 1.0 M HCl solutions at room temperature were carried out using Jeol JSM-7500F scanning electron microscope (SEM). The SEM images were recorded in the vacuum mode before and after immersion time of 24 hours in 1.0 M HCl. The instrument was operated at 15 kV.

2.2.8. Gravimetric Technique

One hundred millilitres (100ml) each of the 1.0 M HCl solution was measured into six different beakers with one as the blank (uninhibited solution) and the remaining five labeled A to E containing different concentrations of the inhibitors ranging from 20 ppm to 100 ppm respectively. One low carbon steel coupon per beaker was used in each experiment. The test coupons were weighed before immersion in the acid solutions and the measurements were taken down. After weighing, the coupons were immersed in the acid solution and then placed in a thermostatic water bath maintained at 303 K. The coupon in each beaker was noted to avoid mix ups during the practical work. The immersion period was two hours intervals after which the coupons were retrieved from the acids solution, washed with tap water, degreased with ethanol and dried with acetone before the corresponding weights after immersion were recorded. The procedures were repeated for ten hours at 313 K, 323 K, 333 K and 343K respectively. The differences in weight of the coupons were again taken as the weight loss [36]. The corrosion rate (CR), inhibition efficiency (IE), and degree of surface coverage (Θ) of mild steel in 1 M HCl solution was computed using the formulas in equation 5 to 7 respectively.

$$\text{Corrosion rat``e (C. R)} = \frac{\Delta W}{A \times T} \quad (5)$$

Where: ΔW = weight loss (g) given as W_o - W_f, W_o is the initial weight and W_f the final weight

A = total surface area of the test coupon (cm^2), T = immersion time (hours).

The Inhibition efficiency (IE) defines the level of performance of inhibitor that causes a decrease in corrosion rate. The inhibition efficiency (IE) was computed using the relationship in equation 6 [37].

$$\%IE = \frac{(C.R)o-(C.R)inh}{(C.R)o} \times 100 \quad (6)$$

Where: $(C.\ R)_o$ and $(C.\ R)_{inh}$ are the corrosion rates in the absence and presence of different concentrations of the inhibitor respectively.

The surface coverage *(θ)* of the inhibitor was obtained from the experimental data using equation 7 as follows:

$$\theta = \frac{(C.R)o-(C.R)inh}{(C.R)o} \quad (7)$$

Where: $(C.\ R)_o$ = Corrosion rate in the absence of inhibitor, $(C.\ R)_{inh}$ = Corrosion rate in the presence of inhibitor.

2.2.9. Electrochemical Measurements

The conventional three electrode set up was used consisting of saturated calomel electrode (SCE) as reference electrode (RE), platinium as counter electrode (CE) and low carbon steel coupons as working electrode (WE). The area of the working electrode exposed to the medium was approximately 1 cm^2. Fresh solution were used after each sweep. Potentiodynamic polarization measurements were carried out to obtain the information regarding the kinetics of the anodic and cathodic reactions on the low carbon steel surface. Before each potentiodynamic polarization (Tafel) study, the electrode was allowed to corrode freely and its open circuit potential (OCP) was recorded as a function of time up to 1 hour, which was sufficient to attain a stable state. After that, a steady-state of OCP corresponding to the corrosion potential (E_{corr}) of the working electrode was obtained. Potentiodynamic polarization studies were conducted from cathodic to the anodic direction on the potential range ±250 mV versus corrosion potential (E_{corr}) at a scan rate of 10 mV/s. Linear polarization resistance

measurements (LPR) were carried out at the potential range ±20 mV with respect to the open circuit potential, and the current response was measured at a scan rate of 0.5 mV/s. This measurement was conducted to support results obtained from PDP measurements. All electrochemical measurements were carried at room temperature.

The inhibition efficiency (%) from PDP was calculated from the measured I_{corr} values using equation (8) [38]:

$$I(\%) = \left(\frac{I^{o}_{corr} - I_{corr}}{I^{o}_{corr}}\right) \times 100 \quad (8)$$

Where I^{o}_{corr} and I_{corr} are the corrosion current densities in the absence and presence of inhibitor respectively. The polarization resistance was obtained using the Stern-Geary equation (1.9).

$$R_p = \frac{\beta_a \times \beta_c}{2.303 \times i_{corr} \times (\beta_a + \beta_c)} \quad (9)$$

Where β_a and β_c are the anodic and cathodic Tafel slopes. From the measured R_p values, the inhibition efficiency (%) was calculated using Equation (10).

$$I(\%) = \left(\frac{R_p - R^{o}_{p}}{R_p}\right) \times 100 \quad (10)$$

Where R^{o}_{p} and R_p are the polarization resistance values in the absence and presence of inhibitors.

The constant phase element which is defined by *Yo* and *n* has correlation with the impedance as follows [39]:

$$ZZ_{CPE} = Y_o^{-1}(j\omega)^{-n} \quad (11)$$

where Y_o is the CPE constant and *n* is the CPE exponent, j= $(-1)^{½}$ which is an imaginary number and ω is the angular frequency in rad/s. CPE was used to compensate for the deviation from ideal dielectric behavior arising from the roughness of the mild steel surface. The value of *n* can be used as a gauge of the heterogeneity or the coarseness of the working electrode surface. The double layer capacitance (C_{dl}) values were calculated from equation (12) expression.

$$C_{dl} = \frac{1}{\omega R_{ct}} = \frac{1}{(2\pi f_{max} R_{ct})} \quad (12)$$

Where ω is the angular frequency ($\omega = 2\pi f_{max}$), f_{max} is the frequency at which the imaginary component of the impedance is maximum. The inhibition efficiency acquired from the impedance spectroscopy measurements was calculated using equation (13):

$$\%IE = \frac{R_{ct(inh)} - R^{o}_{ct}}{R_{ct(inh)}} \times 100 \quad (13)$$

Where $R_{ct(inh)}$ and R^{o}_{ct} are the charge transfer resistance in the presence and absence of inhibitor, respectively.

2.2.10. Adsorption Isotherm

Adsorption isotherm provides information about the adsorbed molecules and their interaction with the metal surface [40]. It is the first step in the inhibition process involving Organic inhibitors. Organic inhibitors act by displacing water molecules from the metal surface followed by interaction with anodic or cathodic sites. Two inhibition mechanisms (physisorption and chemisorption) are generally considered when discussing the adsorption mechanism of organic inhibitor. Physisorption has to do with the electrostatic interaction between charged metal surface and inhibitor species. Chemisorption on the other hand involves the sharing of electron pair. The most frequently used isotherms include: Langmuir, Frumkin, Hill de Boer, Parsons, Temkin, Flory-Huggins, Dhar-Flory-Huggins, Bockris-Swinkels and the recently formulated thermodynamic/kinetic model of El-Awady isotherm [41]. The type of the adsorption isotherm applicable can provide additional information about the properties of the tested compound. All these isotherms are of the general form:

$$f(\theta, x)e^{(-2a\theta)} = KC \quad (14)$$

Here $f(\theta, x)$ represents the configuration factor which depends on the physical model and assumptions underlying the derivation of the particular model. K is the adsorption equilibrium constant which describes how strongly the molecules are held on the adsorbent surface and *a* is the molecular interaction parameter used to predict the nature of interactions in the adsorbed layer. Most of the adsorption isotherms used for corrosion inhibition studies are derived from this general formula and amended to fit certain purpose (s) and assumptions.

3. Results and Discussion

3.1. Physical Properties of the Schiff Base Ligands

The physical properties of the synthesized Schiff bases and its metal complexes were analyzed and presented in Table 1. The Schiff base ligands (SBL1) and its metal complexes were prepared in good yield, coloured and air-moisture stable. The colour changes observed were confirmed by the electronic transition from lower to higher energy level. The melting points of the complexes were higher than that of the ligand (Table 1) indicating that the complexes are thermally more stable than the ligand.

The elemental analysis of these compounds was also carried out in order to resolve the molecular formulae of the complexes. This was achieved by determining the percentages of carbon, hydrogen and nitrogen in the compounds which enabled the comparison of the theoretical and calculated values (Table 1). The micro-analysis data (Table 1) suggested that all the complexes were mononuclear where two moles of the ligand and two moles of water molecules were coordinated to the central metal atom. The data therefore suggested that the metal to ligand ratio in the complex was 1: 2. The values obtained showed a reasonable agreement with the calculated values for the corresponding elements in all the compounds. The data for the Schiff base and its metal complexes suggested the formation of $C_{17}H_{20}N_2O_2$ for SBL1, $[Zn(C_{17}H_{19}N_2O_2)_2(H_2O)_2]$ for ZnL1, $[Ni(C_{17}H_{19}N_2O_2)_2\ (H_2O)_2]$ for NiL1 and $[Cu(C_{17}H_{19}N_2O_2)_2\ (H_2O)_2]$ for CuL1.

Table 1. *Physical Properties of the Schiff Base Ligands.*

Compound	Molecular Formular	Colour	Yield (%)	Melting Point/D. Temp.	Elemental Analysis Calculated (Found)		
					C%	H%	N%
SBL1	$C_{17}H_{20}N_2O_2$ (284.37)	Bronze	74.63	187	71.80 (71.20)	7.04 (6.89)	9.85 (9.42)
ZnL1	$[Zn(C_{17}H_{19}N_2O_2)_2 (H_2O)_2]$ (668.10)	Light Pink	47.30	220	61.07 (61.01)	6.29 (5.78)	8.38 (8.96)
NiL1	$[Ni(C_{17}H_{19}N_2O_2)_2 (H_2O)_2]$ (661.41)	Light Gray	61.50	245	61.69 (62.56)	6.35 (6.28)	8.50 (8.64)
CuL1	$[Cu(C_{17}H_{19}N_2O_2)_2 (H_2O)_2]$ (666.26)	Blank	75.00	270	61.24 (62.50)	6.30 (5.55)	8.41 (9.02)

SBL1= Schiff base ligand (1), D. Temp. = Decomposition Temperature

3.2. Solubility of the Schiff Base Ligands

The solubility of the Schiff base (SBL1) and its metal complexes were determined in different solvents. From the result of solubility test presented in Table 2, it can be observed that, SBL1, ZnL1, NiL1 and CuL1 were soluble in acetic acid, dimethylsulfoxide (DMSO) and dimethylformamide (DMF), slightly soluble in ethanol and methanol, and insoluble in water. SBL1 and its metal complexes (ZnL1, NiL1, and CuL1) were insoluble in acetone.

Table 2. *Solubility of the Schiff Base Ligands.*

Compound	Distilled Water	Methanol	Ethanol	Acetic Acid	Acetone	DMSO	DMF
SBL1	IS	SS	SS	S	IS	S	S
SBL2	IS	SS	SS	S	S	S	S
ZnL1	IS	SS	SS	S	IS	S	S
NiL1	IS	SS	SS	S	IS	S	S
CuL1	IS	SS	SS	S	IS	S	S

S = Soluble, SS = Slightly Soluble, IS = Insoluble

3.3. Molar Conductivity Measurements

The molar conductance values of the synthesized compounds in DMSO 10^{-3} M were measured at room temperature (Table 3). The conductance values of the synthesized compounds were below 50 $\Omega^{-1}cm^2mol^{-1}$ indicating their non-electrolytic nature [42, 43]. This suggested that there were no ions present outside the coordination sphere of the complexes i e, the complexes were neutral.

Table 3. *Molar Conductivity test of the Metal (II) Complexes.*

Complex	Concentration (mol/dm^3)	Specific Conductance (Ω^{-1} cm^{-1})	Molar Conductance (Ω^{-1} cm^2 mol^{-1})
ZnL1	1 x 10^{-3}	8.40 x 10^{-6}	8.40
NiL1	1 x 10^{-3}	12.80 x 10^{-6}	12.80
CuL1	1 x 10^{-3}	15.60 x 10^{-6}	15.60

3.4. Electronic Spectra and Magnetic Susceptibility Studies of the Schiff Base Ligand and Its Metal Complexes

The electronic absorption spectra also known as the ultra-violet visible spectra is a useful tool for the evaluation of results provided by other methods of structural investigation. It is used to designate the stereochemistry of the metal ions in a complex as shown by the positions and numbers of d-d transition peaks. The structure of the schiff base and its complexes was elucidated by the absorption bands they exhibited. The electronic spectral data of the Schiff base (SBL1) and its complexes are shown in Table 5. SBL1 showed two major bands at 238.5 nm (41928.72 cm^{-1}) and 306 nm (32679.74 cm^{-1}) (Figure 1). The band appearing at lower energy (306 and 320.5 nm) is attributed to n – π^* transition as a result of the nonbonding electrons present on the nitrogen atom of the azomethine group (-HC=N) and the phenolic group. The band appearing at higher energy (238.5, 249.5 and 275.0 nm) is due to $\pi - \pi^*$ transition of the ligand centered transitions (LCT) of benzene ring [44, 45].

The electronic spectra of Zn (II) complex shows absorption band at 361 nm (27700.83 cm^{-1}) for SBL1 complex due to charge transfer transition from the metal to the ligand (M→L). No d –d transitions are observed for the complexes due to its complete d^{10} electronic configuration. The observed magnetic moment values for these complexes are zero, indicating diamagnetic nature of the complexes (Table 4). On the basis of analytical, conductance and spectral data, octahedral geometry was proposed for the zinc complexes [46-48].

The electronic spectrum of Ni (II) complex in Schiff base ligand 1 (SBL1) showed that the bands shifted to the red with three bands at 354 nm (28248.59 cm^{-1}), 360.50 nm (27739.25 cm^{-1}) and 634.50 nm (15772.87 cm^{-1}) for SBL1 complexes were attributed to the d-d transition of $^3A_{2g}$ (F) → $^3T_{2g}$ (F) and $^3A_{2g}$ (F) → $^3T_{1g}$ (F), and the charge transfer transition of $^3A_{2g}$ (F) → $^3T_{1g}$ (P) respectively, which favours an octahedral geometry for the Ni (II) complex [47, 49]. The magnetic moment value of Ni (II) complex was found to be 2.84 BM,

fell within the range of 2.8 – 3.5 BM for octahedral complexes, and suggested octahedral geometry (Table 4).

Copper (II) complex spectrum showed two bands at 229.1 nm, and 349.7 nm (Figure 5), which was a red shift. The bands at 352 nm and 494 nm for SBL1 complexes. 352nm and 335nm were due to intra-ligand transition and the one at 392 nm and 494 nm was as a result of d-d spin allowed transition for $^{2}E_{g}$ (D) → $^{2}T_{2g}$ (D) indicating octahedral geometry around Cu (II) ion and finally the fourth absorption band ranging 650 – 765 nm in any of the complexes indicated the presence of water [50]. The observed magnetic value of Cu (II) was 1.73 BM (SBL1 complexes) which fell within the expected range observed for octahedral geometry. The absence of any band below 118nm eliminates the possibility of a tetrahedral environment in these complexes [51]. It was also concluded that a shift in the spectra of the complexes, with respect to the spectrum of the Schiff base ligand, bathochromically or hypsochromically, indicated coordination.

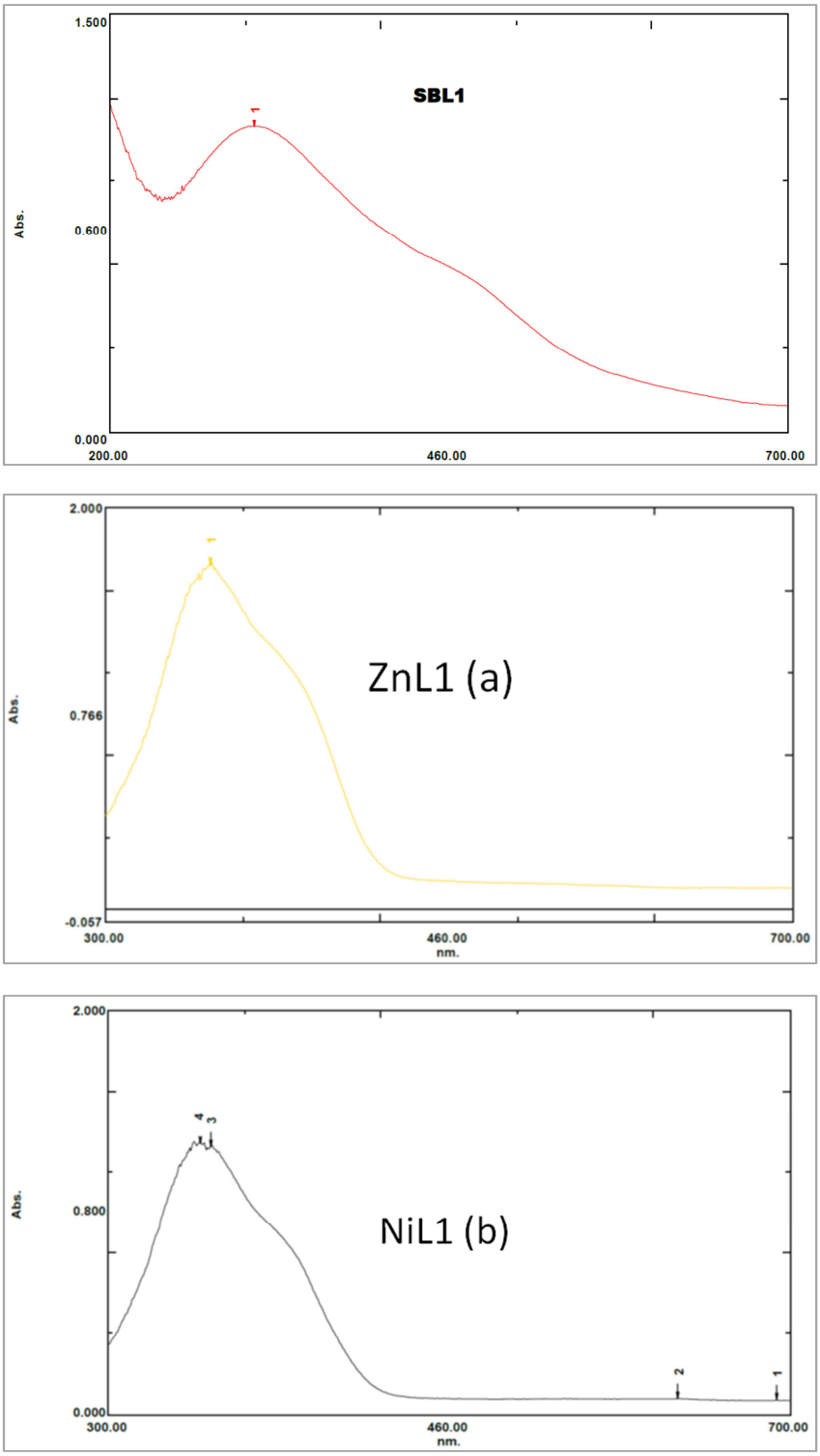

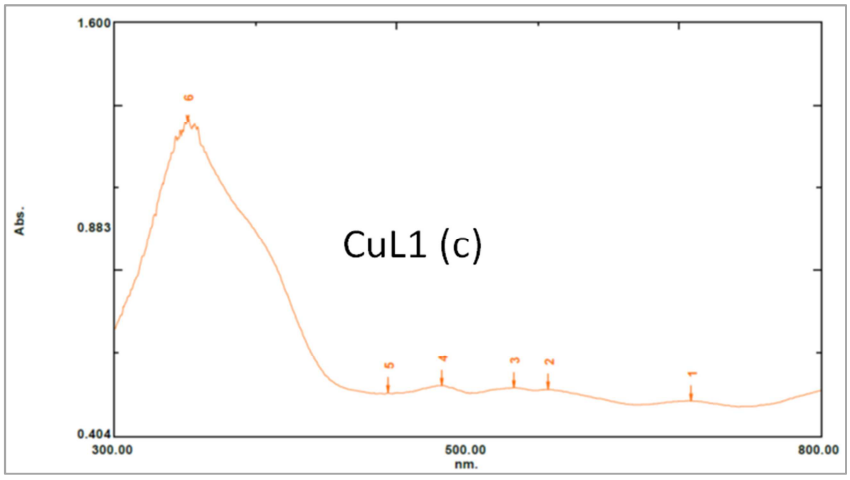

Figure 5. *Electronic spectra of SBL1, (a) ZnL1, (b) NiL1, (c) CuL13.5.*

Table 4. *Magnetic Susceptibility value of the Metal (II) Complexes.*

Complex	Mass Susceptibility, χ_g ($cm^3\ g^{-1}$)	Molar Susceptibility, χ_m (mol^{-1})	μ_{eff} (BM)	Suggested Structure
$[Zn(C_{17}H_{19}N_2O_2)_2\ (H_2O)_2]$	-36.80 x 10^{-6}	-23.82 x 10^{-3}	Diamagnetic	Octahedral
$[Ni(C_{17}H_{19}N_2O_2)_2\ (H_2O)_2]$	5.13 x 10^{-6}	3.38 x 10^{-3}	2.84	Octahedral
$[Cu(C_{17}H_{19}N_2O_2)_2\ (H_2O)_2]$	1.94 x 10^{-6}	1.25 x 10^{-3}	1.73	Distorted Octahedral

Table 5. *Electronic Spectroscopic Data for the Schiff base Ligands.*

Compound	λ_{max}	Absorption, ν (cm^{-1})	Transition
SBL_1	238.5	41928.72	$\pi \rightarrow \pi^*$
	306.0	32679.74	$n \rightarrow \pi^*$
ZnL1	361	27700	CT
	354	28248.59	ILT
NiL1	361	27739.25	$^3A_{2g}\ (F) \rightarrow {}^3T_{2g}\ (F)$
	634	15772.87	$^3A_{2g}\ (F) \rightarrow {}^3T_{1g}\ (F)$
	693	14440.43	$^3A_{2g}\ (F) \rightarrow {}^3T_{1g}\ (P)$
	352	28409.10	ILT
CuL1	494	20242.92	$^2E_g\ (D) \rightarrow {}^2T_{2g}\ (D)$
	708	14124.29	

3.5. FT-IR Spectral Analysis

The binding mode of the Schiff base ligand to the metal ions in the complexes was studied by comparing the FT-IR spectrum of the free ligand with the spectra of the complexes. The FT-IR data of the ligand and its metal (II) complexes together with assignments for most of the major peaks (Figure 6) were given in Table 6 below.

Table 6. *The Relevant Infrared Spectra Data for the Schiff base Ligands, its Complexes and the corrosion of the Schiff bases.*

Compound	C-H	C--C	C-O	C-N	C=N	O-H	H_2O	M - N	M - O
SBL1	2097	1439	1327	1088	1580	3250	671.3	-------	------
ZnL1	2924	1481	1335	1150	1636	3403	671.3	594.1	475.2
NiL1	2924	1397	------	1142	1643	3403	671.3	594.1	478.4
CuL1	2924	1489	1404	1150	1643	3403	671.3	609.5	470.7
SBL1 + MS	2922	1424	1329	1088	1625	3161	790.2	-------	-------

SBL1 = Schiff base ligand 1, Sbl2 = Schiff base ligand 2, MS = Mild steel

The azomethine vibration (C=N) of the free ligand at 1617.70 - 1580.40 cm^{-1} region was shifted to higher wave numbers (1643 – 1636 cm^{-1}) after complexation (Figure 2). This indicated coordination of Schiff base through the azomethine nitrogen [52]. Moreover, the appearance of additional weak bands in the region 609.5 – 594.1 cm^{-1} and 501.5 – 470.7 cm^{-1} (Table 6) attributed to (M-N) and (M-O), respectively [53], further confirmed complexation [54]. This showed that the Schiff base ligand coordinated to the metal via "N" and "O" atoms. C-C occuring in the region 1438.80 -

1416.40 cm^{-1} in the free ligands shifted to 1505 – 1397 cm^{-1}, C-N occuring in the region 1088.40 - 1080.90 cm^{-1}, shifted to 1157 – 1142 cm^{-1}, C-H stretching occuring in the region 2937.10 –2097.30 cm^{-1} shifted to lower wave numbers. This was also attributed to the coordination of the ligands to metal through the O and N atoms. The FT-IR spectra of the complexes also showed strong bands at 3403 cm^{-1} region (Table 6), suggesting the presence of coordinated/lattice water in the complexes. That was further confirmed by the appearance of non-ligand band in 671.3 cm^{-1} region, assignable to the rocking mode of water [54]. In the free Schiff base ligand, the band occurring at 1326.9 cm^{-1} due to υ(C-O, phenolic) shifted to higher wave number (1404 – 1327 cm^{-1}) in the complexes indicating the coordination of the phenolic oxygen atom to the metal ion [55]. Therefore it was be concluded that coordination took place via phenolic oxygen and azomethine nitrogen of the Schiff base ligand molecule.

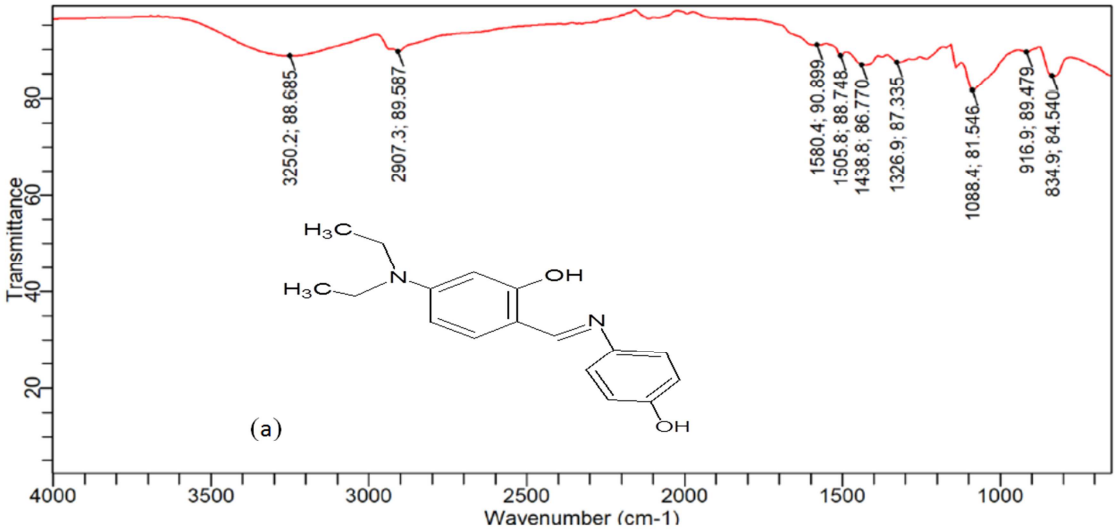

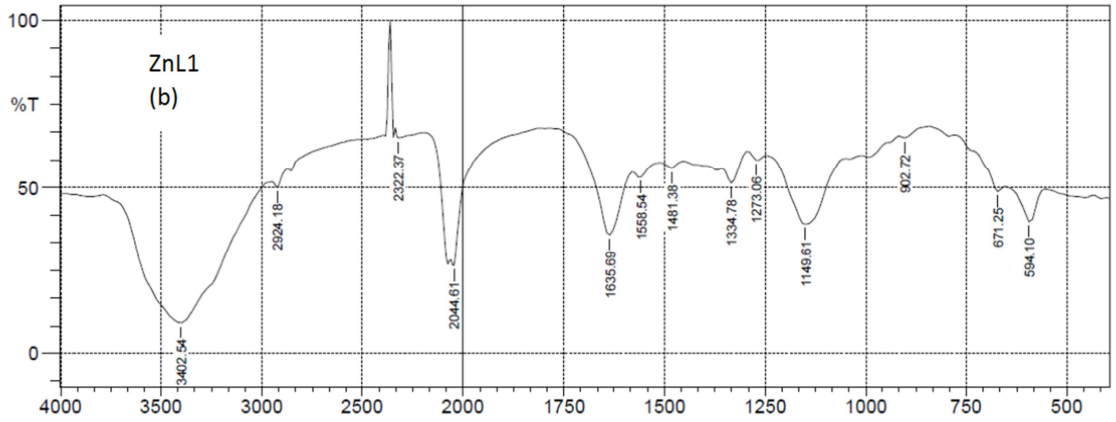

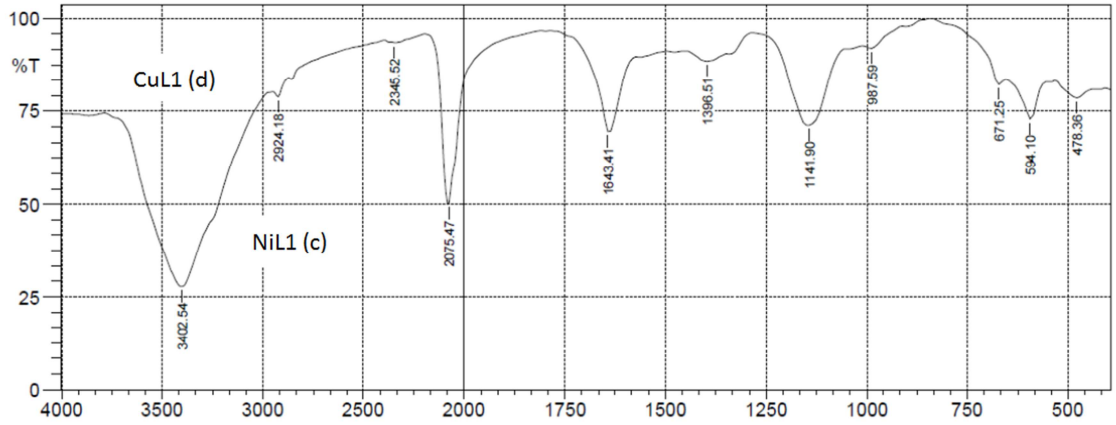

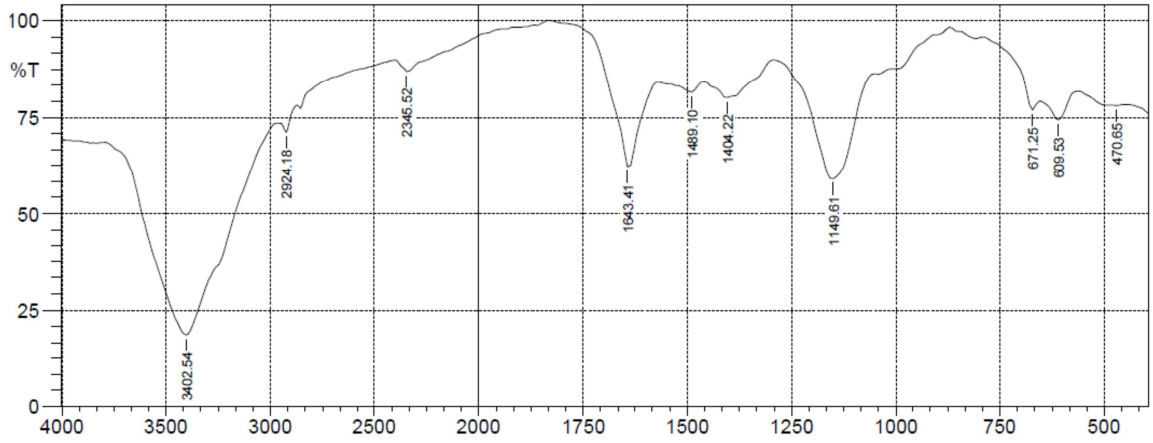

Figure 6. *FTIR spectra of (a) SBL1 (b) ZnL1, (c) NiL1, (d) CuL1.*

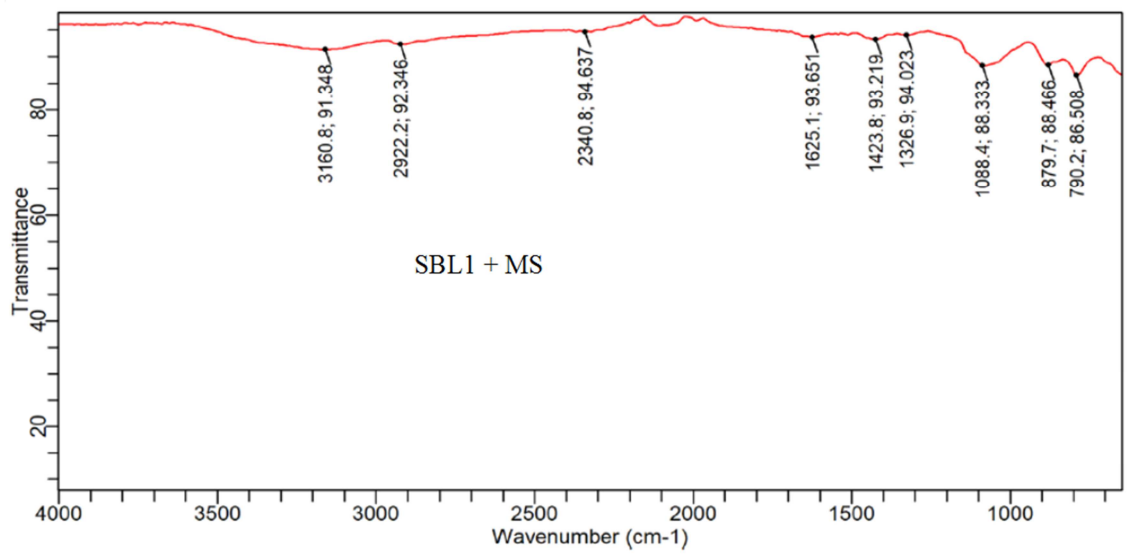

Figure 7. *FTIR spectra of the corrosion products of mild steel in the presence of SBL1and in 1 M HCl acid.*

Furthermore, FTIR analysis was also used to ascertain the fact that the corrosion inhibition process took place through the adsorption of the Schiff base (SBL1) on the low carbon steel surface. The infrared absorption spectra of the Schiff base and their corrosion products are presented in Table 6. by comparing the FT-IR spectrum of the free Schiff base ligand (Figure 6) with the spectra of the corrosion product in the presence of SBL1 (Figure 7), functional groups responsible for adsorption were deduced. The spectra of the Schiff base as well as scraps from the inhibitors films on the surface of the metal are presented in Figures 6 and 7. From the results obtained, the azomethine stretch (C=N) at 1580.4 cm^{-1} shifted to 1625.1 cm^{-1}, C–O stretch at 1326.9 cm^{-1} shifted to 1328.9 cm^{-1}, C–C bend at 834.90 cm^{-1} shifted to 879.7 cm^{-1}, C–C stretch at 1438.8 cm^{-1} shifted to 1423.8 cm^{-1}, C-H stretch at 2097.3 cm^{-1} shifted to 2922.2 cm^{-1}, C-N stretch at 1088.4 cm^{-1} shifted to 1095.8$cm^{-1}$and O–H stretch at 3250.2 cm^{-1} shifted to 3160.8 cm^{-1}. The shifts in frequencies indicated that there was an interaction between the mild steel surface and the Schiff base. On the other hand, C=C stretch at 1505.80 cm^{-1}, and C-H stretch at 2064.90 cm^{-1} were missing in the spectrum of the corrosion products, suggesting that these functional groups were used for the adsorption of the inhibitor onto the surface of the low carbon steel [56]. Also, some new bonds were found in the spectrum of the corrosion product. These included the C-H stretch at 2340.80 cm^{-1}, C-N stretch at 1006.4 cm^{-1} and C-H bend at 790.2 cm^{-1}. This also indicated that some new bonds were also formed through these functional groups [56]. The presence of these functional groups indicated the effectiveness of the Schiff base to interact with the low carbon steel surface and that adsorption between the Schiff base and the low carbon steel occured through the identified functional groups [57]. Hence, protection of metallic surface was done via the functional groups presented in the Schiff base (SBL1).

3.6. Gravimetric Measurements

Figure 8. indicated that the Schiff base and its metal complexes (SBL1, ZnL1, CuL1 and NiL1) indeed inhibited the corrosion of low carbon steel in 1 M hydrochloric acid solution since there was a general decrease in corrosion rate at the end of the corrosion monitoring process at different

time interval. This may be ascribed to the adsorption of inhibitor on the low carbon steel surface, producing a barrier which isolated the surface from the corrosive environment. However, there was a progressive increase in corrosion rate of SBL1 compared to the metal complexes, and the trend followed SBL1>ZnL1>CuL1>NiL1. Figure 9 also showed that the inhibition efficiencies of the Schiff base and its metal complexes in the test solutions increased with increase in concentrations of the inhibitor. Conversely, the inhibition efficiency of the metal complexes tended to be higher than SBL1 with NiL1 having the maximum concentration at the various concentrations under review. Furthermore, the inhibition efficiency of NiL1 was estimated to be 53.84% even at low concentration (20 ppm) and reached 88.46% at a concentration of 100 ppm. This behaviour was due to the fact that the adsorption coverage of NiL1 inhibitor on metal surface increased with the inhibitor concentration. Such remarkable performances may be due to, the high molecular weight and the presence of abundant electron donation groups (C=N, O-H, C-N, N=N and aromatic rings).

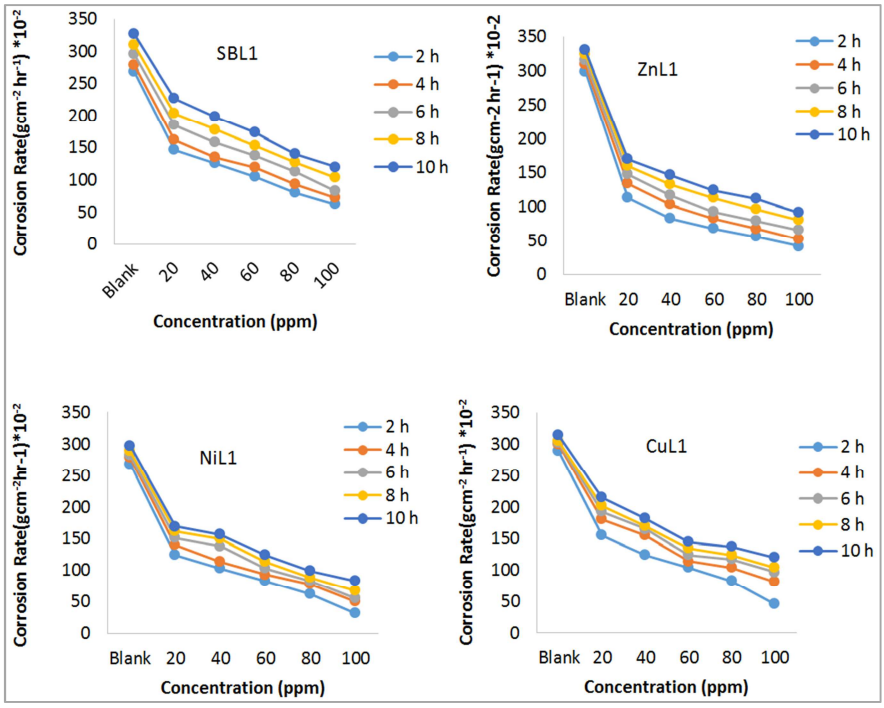

Figure 8. *Variation of corrosion rate with concentration for mild steel coupons in 1 M HCl solution containing SBL1, ZnL1, NiL1 and CuL1 at different time intervals.*

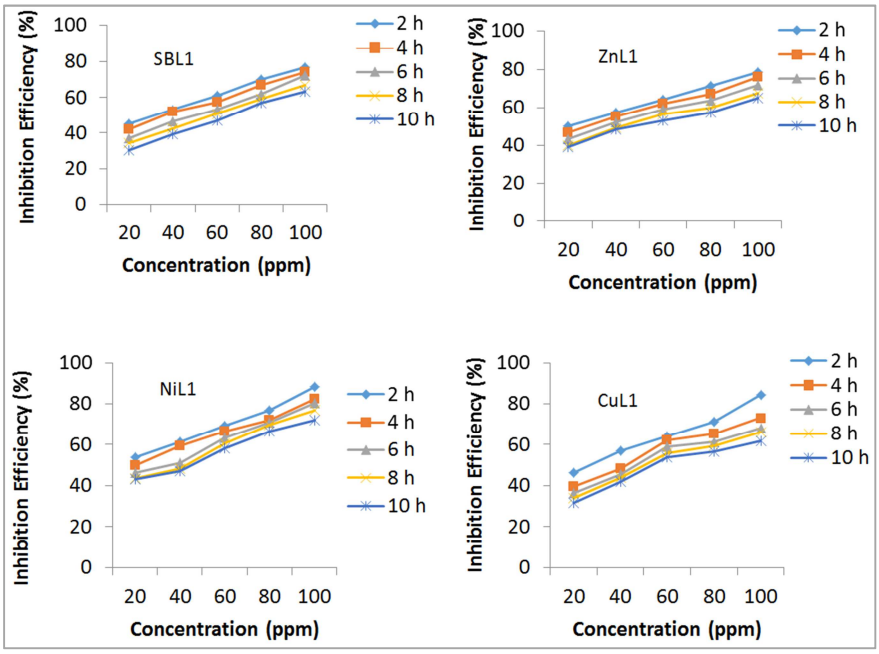

Figure 9. *Variation of inhibition efficiency with concentration of SBL1, ZnL1, NiL1 and CuL1 at different time intervals.*

3.7. Effect of Temperature

Lately, some industries have dabbled into1 the production and recovery of hydrocarbons from deep pay zones. A significant variable that may affect the efficacy of the corrosion inhibitor in such operations is the difference between surface and down-hole temperatures. The difference when going down the well is known as geothermal gradient, defined as a change in temperature per unit length of well. Geologists estimate that the average geothermal gradient across the globe is about 25°C per km of depth (1°F per 70 feet) [2, 58].

Using gravimetric measurement, the highest concentration of the inhibitor was tested at five different temperatures ranging from 303 K to 343 K to clarify the impact of temperature on the performance of the Schiff base. Results obtained (Table 7) clearly showed that the inhibition efficiency decreased gradually as temperature increased. The decrease seemed reluctant from 303 K to 323 K but became more prominent at higher temperatures. This implies that Schiff base would perform effectively at surface conditions but loose its efficiency some kilometers down the well. In literature, this trend was associated with desorption of reversibly physisorbed inhibitor molecules at an increased temperature [59]. To improve the efficiency of Schiff base at high temperatures, the Schiff base ligand was blended with transition metal such as zinc (Zn), nickel (Ni) and cupper (Cu) forming metal complexes. The metal complexes are known for its synergistic enhancement of corrosion inhibition effect [60-61]. Other metal complexes have been reported to inhibit corrosion [62-63]. The results obtained (Table 7) showed that the inhibition efficiency improved at high temperatures. This demonstrated that the metal complexes could be more efficient in various oilfield acidizing procedures associated with high temperature operations. Similar results (Table 8) were obtained using electrochemical measurements.

Table 7. *Effect of Temperature on the Inhibition Efficiency (%) of Schiff base and its metal complexes after 2 h at 20 and 100 ppm.*

Concentration (ppm)	Temperature, K	Schiff base	ZnL1	NiL1	CuL1
20	303	45.39	50.00	53.84	46.43
	313	42.22	46.15	50.00	35.72
	323	39.85	42.31	46.67	28.57
	333	36.03	40.74	42.85	26.66
	343	33.10	34.78	38.46	23.33
100	303	76.92	78.57	88.46	84.29
	313	71.85	76.92	85.71	78.57
	323	69.92	73.08	80.00	71.43
	333	66.91	70.37	78.57	66.66
	343	64.79	67.39	76.92	63.33

3.8. PDP and LPR Measurements

Potentiodynamic polarization measurements were performed in order to examine the effect of addition of Schiff base and its metal complexes (SBL1, ZnL1, NiL1 and CuL1) on the corrosion of low carbon steel in 1 M HCl.

Table 8. *PDP parameters for low carbon steel corrosion in 1 M HCl containing different concentrations of SBL1, ZnL1, NiL1 and CuL1.*

compound	Concentration (ppm)	-E_{corr}(mV)	I_{corr} (µA)	β_c (V/dec)	β_a (V/dec)	η%
	Blank (1M HCl)	472	905	65.10	113.70	---------
SBL1	20	480	815	102.30	111.30	9.95
	100	486	689	105.50	124.20	23.87
ZnL1	20	493	651	101.90	100.80	28.07
	100	500	518	124.50	106.90	42.76
NiL1	20	479	459	103.90	96.60	49.28
	100	493	121	115.50	105.50	86.63
CuL1	20	485	623	96.90	89.60	31.16
	100	496	452	130.50	122.30	50.06

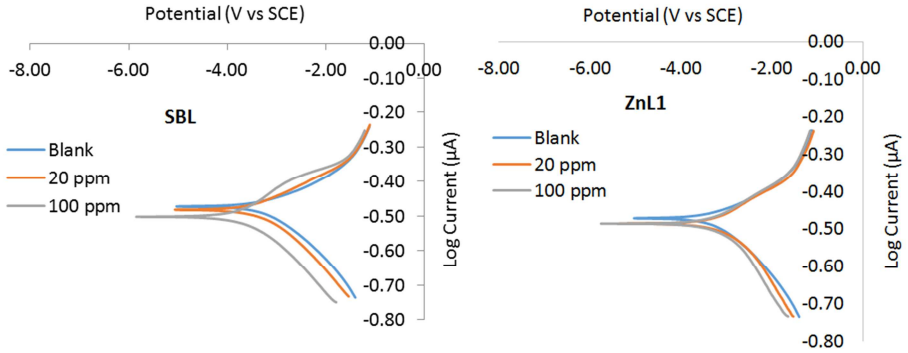

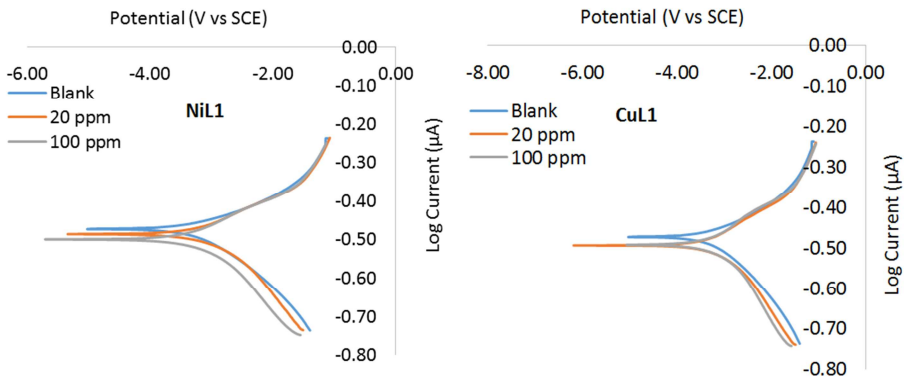

Figure 10. *Tafel plots for low carbon steel corrosion in 1 M HCl containing different concentrations of SBL1, ZnL1, NiL1 and CuL1.*

Figure 10. present the Tafel curves for low carbon steel in 1 M HCl solution in the absence and presence of the Schiff base and its metal complexes. Low carbon steel however, involves a mixture of many metals, a number of oxidation reactions may occur at the anode. The various anodic oxidation reactions may be represented in Equation (15) while the oxidation of iron in the steel sample may be represented by Equation (16).

$$\text{Anode: } M_{(s)} \rightarrow M_{(aq)}^{n+} + ne^- \quad (15)$$

$$Fe_{(s)} \rightarrow Fe_{(aq)}^{2+} + 2e^- \quad (16)$$

The reaction at the anode could involve reduction of water in aqueous environments with sufficiently negative potential (Equation 17) and subsequent evolution of hydrogen (Equaqtion 18).

$$\text{Cathode: } H_2O + e^- \rightarrow H^+ + OH^- \quad (17)$$

$$2H_{(aq)}^+ + 2e^- \rightarrow H_{2(g)} \quad (18)$$

The potential served as the driving force and was controlled to measure the current as a function of the net change in reaction rate. The sum of currents resulting from the electrode processes can be used to obtain the free corrosion current density (I_{corr}) and the corresponding potential (E_{corr}). The potentiodynamic polarization parameters including corrosion current density (I_{corr}), potential (E_{corr}), cathodic and anodic constants (β_c and β_a) and inhibition efficiency (%) are presented in Table 8. The I_{corr} values decreased with an increase in inhibitor concentration compared to the free acid solution. This was due to formation of adsorbed protective film of the Schiff base and its metal complexes (SBL1, ZnL1, NiL1 and CuL1) on low carbon steel surface. A displacement of E_{corr} to less negative values in the inhibited solutions compared to the free acid solution was also observed (Figure 10). Corrosion inhibitors that displace E_{corr} to less negative values are usually identified as anodic inhibitors whereas cathodic inhibitors displace the potential to more negative values [64, 65]. Consequently, the E_{corr} values obtained suggested that the inhibitors (SBL1, ZnL1, NiL1 and CuL1) have dominant influence on the partial anodic and cathodic reaction. However, NiL1 showed greater influence compared to SBL1, ZnL1 and CuL1. Thus, the addition of the Schiff base and its metal complexes further shifted the corrosion potential (E_{corr}) towards negative values but the shift was not up to - 85 mV/SCE to categorize the Schiff base inhibitors as cathodic or anodic type. Such corrosion inhibitors are usually regarded as mixed type inhibitors with anodic predominance [12, 66]. The values of β_c and β_a obtained change on addition of inhibitor from that of the free acid solution (Table 8). The highest difference was obtained with β_a supporting that the Schiff base and its metal complexes (SBL1, ZnL1, NiL1 and CuL1) exhibited greater influence on anodic reaction than cathodic reaction. A mixed type inhibitor acts by blocking some active anodic and cathodic sites of the metal without changing its dissolution or corrosion mechanism. In other words, Schiff base and its metal complexes (SBL1, ZnL1, NiL1 and CuL1) inhibited both the iron dissolution and hydrogen evolution processes, but more actively inhibiting iron oxidation (anodic reaction). The calculated inhibition efficiency also increased with increase in concentration of the inhibitor.

Table 9. revealed that values of R_p increased in the presence of the studied inhibitors. The results also showed that R_p values increased with increase in the concentration of the Schiff base and its metal complexes (SBL1, ZnL1, NiL1 and CuL1). The inhibition efficiency obtained from polarization resistance followed the same trend as PDP with respect to concentration. However, inhibition efficiency obtained were relatively higher than those from PDP measurements.

Table 9. *LPR parameters for low carbon steel corrosion in 1 M HCl containing different concentrations of SBL1 and its metal complexes.*

compound	Concentration (ppm)	R_p (Ωcm^2) x 10^{-2}	η%
	Blank (1M HCl)	1.1179	-----
SBL1	20	2.8147	60.28
	100	3.5249	69.16
ZnL1	20	3.3805	66.93
	100	4.8216	76.82
NiL1	20	4.7357	58.15
	100	1.9786	89.98
CuL1	20	3.2430	65.53
	100	6.0631	81.56

3.9. Adsorption and Thermodynamic Considerations

The mode and extent of the interaction between each of the inhibitors (SBL1, ZnL1, NiL1 and CuL1) and the metal surfaces were studied by applying adsorption isotherms.

Surface coverage values (η%/100) from weight loss data were theoretically fitted into different adsorption isotherms and the best fit was adjudged by the value of the linear regression coefficient (R^2) (Table 10). The Langmuir thermodynamic–kinetic adsorption isotherm [67] given by Equation (19) gave the best fit.

$$\frac{C}{\theta} = \frac{1}{K_{ads}} + C \quad (19)$$

Where K_{ads} is the equilibrium constant of adsorption, C is the concentration of the inhibitors. K_{ads} is related to the standard free energy of adsorption ($\Delta G°_{ads}$) by the equation as follows:

$$\Delta G°_{ads} = - RTIn(55.5K_{ads}) \quad (20)$$

Where 55.5 is the molar concentration of water molecules expressed in g/L, R is the universal gas constant and T is the absolute temperature. Negative values of ΔG_{ads} showed that the inhibitor molecules were spontaneously adsorbed on the metal surface. The mechanism of adsorption is physisorption when the value of $\Delta G_{ads} \leq$ - 20 kJmol^{-1} and chemisorption when $\Delta G_{ads} \geq$ -40kJmol^{-1} [68]. In all cases, straight line graphs were obtained indicating that the experimental data fitted well into Langmuir adsorption isotherm model (Figure 11). The adsorption parameters deduced from the linear graph are listed in Table 10. The values of $\Delta G°ads$ were found to be negatively less than the threshold value of −40 kJ mol^{-1} required for the mechanism of chemical adsorption. This indicated that the adsorption of the studied Schiff base and its metal complexes (SBL1, ZnL1, NiL1 and CuL1) on the low carbon steel surface was spontaneous and consistent with the mechanism of physical adsorption [69 -71].

Table 10. *Isotherm parameters for the adsorption of SBL1 and its metal complexes on the surface of low carbon steel in HCl at 303 K.*

Compound	K_{ads}	ΔG_{ads} (KJmol^{-1})	R^2
SBL1	34.483	-19.040	0.975
ZnL1	43.370	-19.620	0.982
NiL1	43.480	-19.630	0.966
CuL1	34.48	-19.040	0.962

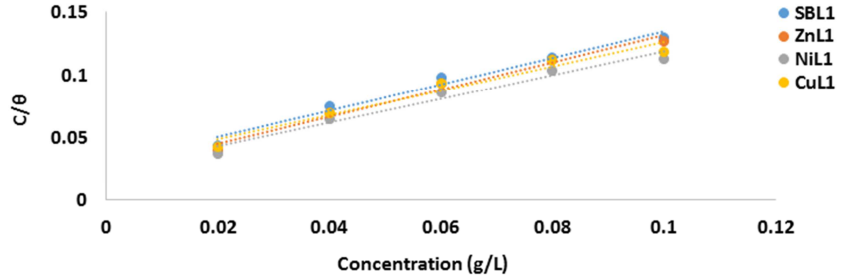

Figure 11. *The Langmuir isotherm for the adsorption of SBL1, ZnL1, NiL1 and CuL1 on mild steel surface in 1.0 M HCl at 303 K.*

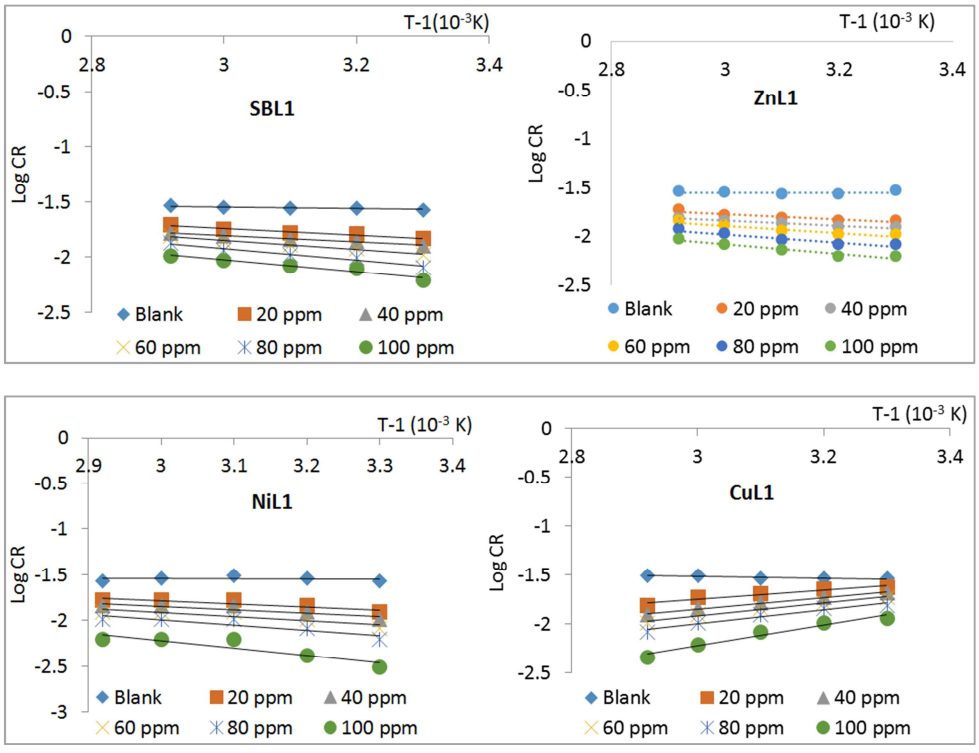

Figure 12. *Arrhenius Plot of log CR against T^{-1} for mild steel in 1 M HCl solution in the absence and presence of various concentrations of SBL1, ZnL1, NiL1 and CuL1.*

Thermodynamic parameters also provide useful insights into the inhibitive mechanism of the inhibitors [72]. The rate of corrosion increased with increasing temperature for all tested systems. The activation energy was determined from linear plots of logCR against the reciprocal of temperature (Figure 12), which were elucidated by fitting the corrosion rate data into the Arrhenius kinetic model (Equation 21). Depending on the concentration of the inhibitors, the obtained activation energy increased on addition of the inhibitors (Table 11). According to the principle of activation and collision theory, it may be assumed that before the acid solution corrodes the metal surface, acid molecules must collide with the surface-bound metal molecules. This suggested that corrosion inhibition occurred because the HCl molecules under study require additional (higher) energy in the inhibited solution. The increase in activation energy in the presence of inhibitor in 1 M HCl acid was consistent with trends reported in literature and related to the physical adsorption mechanism [2].

$$logCR = logA - \frac{E_a}{2.303RT} \quad (21)$$

The parameter A is the frequency factor or pre-exponential factor which correspond to the intercept of the line at 1/T = 0, It is a measure of the rate at which collisions occur irrespective of their energy and E_a, obtained from the slope of the line (Ea/R), is called the activation energy [73].

Table 11. *Calculated values of thermodynamic and kinetic parameters for mild steel corrosion in 1 M HCl in different concentration of the inhibitors.*

Inhibitor	Concentration (ppm)	A (s^{-1})	E_a (kJ/mol)	$\Delta S°_{ads}$ ($Jmol^{-1} K^{-1}$) x 10^1	$\Delta H°_{ads}$ ($kJmol^{-1}$)
SBL1	Blank	0.05	1.55	-27.89	1.11
	20	0.16	5.96	-26.98	3.18
	40	0.12	5.53	-27.20	2.85
	60	0.26	8.04	-26.52	5.36
	80	0.47	10.15	-26.03	7.47
	100	0.39	10.32	-26.18	7.64
ZnL1	Blank	0.03	0.03	-28.08	1.76
	20	0.09	5.17	-27.52	2.49
	40	0.12	5.44	-27.37	2.76
	60	0.19	7.39	-26.84	4.61
	80	0.20	8.18	-26.74	5.50
	100	0.32	9.47	-26.55	6.79
NiL1	Blank	0.03	0.10	-28.33	2.57
	20	0.16	6.22	-26.95	3.54
	40	0.20	7.26	-26.75	4.58
	60	0.29	8.73	-26.44	6.05
	80	0.53	10.94	-26.93	8.25
	100	0.57	15.74	-24.92	13.06
CuL1	Blank	5.62×10^{-2}	1.71	-27.77	0.88
	20	0.07×10^{-2}	9.04	-25.82	6.45
	40	0.03×10^{-2}	10.97	-25.96	6.61
	60	0.01×10^{-2}	12.60	-25.58	8.03
	80	0.07×10^{-3}	13.69	-24.78	11.19
	100	0.04×10^{-4}	20.15	-23.09	17.73

The values of entropy of activation (ΔS^o_{ads}) and enthalpy of activation (ΔH^o_{ads}) also presented in Table 11 were obtained from the alternative formulation of the Eyring transition state equation (equation 22) [74, 75].

$$log\frac{CR}{T} = \{log\frac{R}{N_A h} + \frac{\Delta S_{ads}}{2.303R}\} - \frac{\Delta H_{ads}}{2.303RT} \quad (22)$$

Where *CR* is the corrosion rate of the metal, h is Plank's constant, N is Avogadro's number, R is the universal gas constant and T is the absolute temperature. A plot of log CR/T against 1/T gives straight lines with slopes (ΔH_{ads}/2.303R) and intercepts [log(R/Nh) + (ΔS_{ads}/2.303R)].

The transition-state equation relates the activation parameters viz; ΔH_{ads} and ΔS_{ads} to corrosion rate of the metal coupons [76]. Linear plots of log CR/T against reciprocal of the temperature were obtained and displayed in Figure 13, and from the slope and intercept of such plots, values of ΔH^o_{ads} and ΔS^o_{ads} were obtained. The positive values of ΔH^o_{ads} denoted the endothermic nature of the corrosion inhibition process. The negative values of ΔS^o_{ads} as shown in Table 11, indicated decreasing disorderliness at the mild steel-inhibitor interface as concentrations of the Schiff bases and their metal complexes increased.

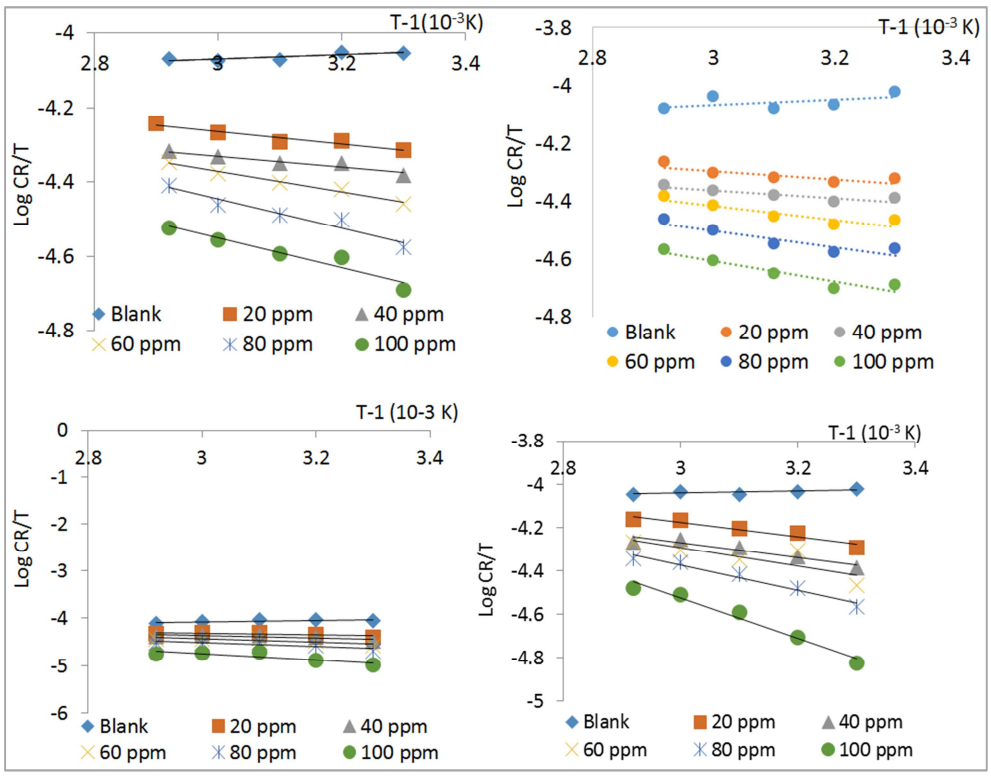

Figure 13. *Transition State Plot of log CR/T against 1/T for mild steel in 1 M HCl solution in the absence and presence of various concentrations of SBL1, ZnL1, NiL1 and CuL1.*

3.10. Surface Studies by Scanning Electron Microscopy

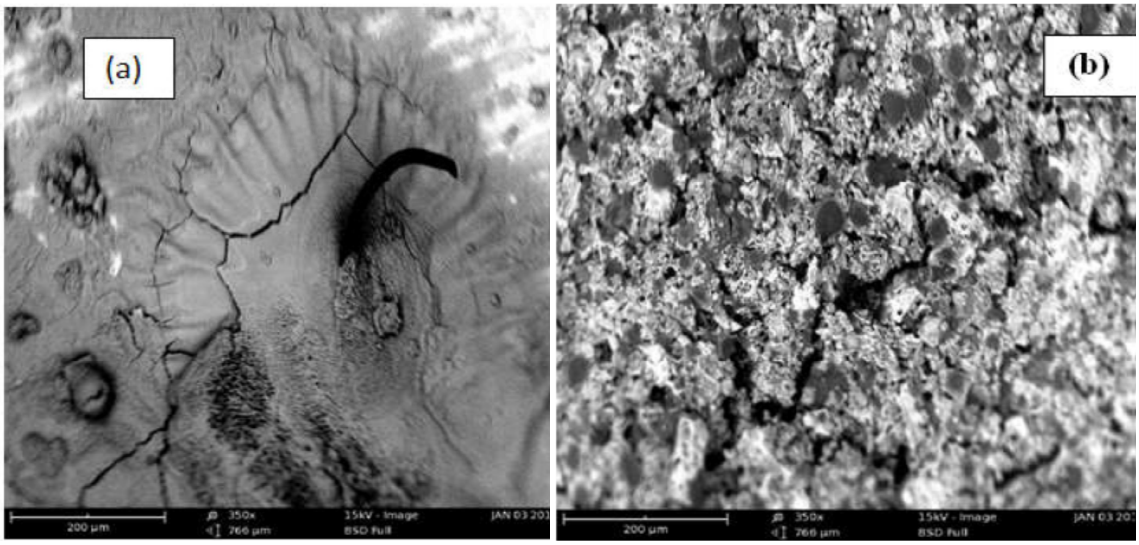

Figure 14. *(a) SEM of the low carbon steel immersed in 1 M HCl solution without inhibitor for 24 h at 200 magnification and (b) SEM of the low carbon steel immersed in 1 M HCl solution in the presence of the Schiff base (SBL1).*

Morphological analysis using SEM showed differences in the morphologies of the samples for both the inhibited and uninhibited media. Figure 14. Shows the SEM image of the mild steel surface immersed in the uninhibited medium for 24 h. The pitting and cracks observed on the surface of the low carbon steel were due to corrosive attack on the specimen in the free acid solution. Similar image of low carbon steel immersed in the inhibited medium is shown in Figure 14. Smoother surfaces with little cracks observed were due to the formation of a thin film layer infused by the complexation between the low carbon steel and the Schiff base (SBL1). This implied corrosion rate was lowered by the Schiff base ligand in agreement with the results obtained from the weight loss analysis.

4. Conclusion

Schiff base and its metal complexes as ecofriendly

pitting corrosion inhibitors on ASTM-A36 low carbon steel in corrosive oil and gas well treatment fluids were successfully investigated. The corrosive fluid was simulated using 1 M HCl solution. From the above results and discussions, it was concluded that the studied Schiff base ligand (SBL1) acted as effective corrosion inhibitor for low carbon steel in 1M HCl acid solution and their inhibition efficiency increased with increase in concentration of the Schiff base with maximum efficiency obtained at an optimum concentration of 100 ppm within the first 2 hours. Complexes of Schiff base formed with zinc, nickel and copper (ZnL1, NiL1 and CuL1) improved the efficiency to values above 76.92 % at 303 K, enhancing its synergistic effect of corrosion inhibition. The UV-Visible, FT-IR and the elemental analysis were employed to confirm the proposed structure of the Schiff bases. The molar conductivity of the metal complexes revealed its non-electrolytic nature. Schiff base and its metal complexes behaves as mixed type inhibitor with anodic predominance. It inhibited ASTM-A36 low carbon steel corrosion by formation of protective film facilitated by benzene rings with delocalised π-electrons, electron rich substituents ($–NO_2$, –Cl, and –OH groups) and the presence of azomethine group (–C=N–) functionalities. Schiff base and its metal complexes were spontaneously, endothermically and physically adsorbed on ASTM-A36 low carbon steel surface and the adsorption was best approximated by the Langmuir adsorption model. Complexes of Schiff base formed with zinc, nickel and copper (ZnL1, NiL1 and CuL1) could be useful as effective alternative ecofriendly corrosion inhibitors for ASTM-A36 low carbon steel materials in acidic well treatment fluids containing HCl. Surface morphology studied by SEM and Fourier transform infrared spectroscopy (FTIR), all indicated that Schiff base and its metal complexes protected ASTM-A36 low carbon steel from the corrosive HCl solution.

References

[1] Odewunmi, N. A, Mazumder, M. A. J, Mohammed, K. A,. and Ali, S. A. (2021). N1, N1, N12, N12-Tetramethyl-N1, N12-dioctyldodecane-1, 12-diaminium bromide: Its synthesis and application in inhibition of mild steel corrosion in 15% HCl. *Journal of Molecular Liquid.* 338: 116630.

[2] Ituen, E. B, James A. O and O. Akaranta. (2016). Fluvoxamine-based corrosion inhibitors for J55 steel in aggressive oil and gas well treatment fluids. *Egyptian Journal of Petroleum.* 6 (2), 1–12.

[3] Ugi, B. U, Mbang, E. O, Victoria, M. B, Louis, H, Stephen, A. A, and Chijioke E. O. (2022). Adsorption and Inhibition Analysis of Aconitine and Tubocurarine Alkaloids as Eco-friendly Inhibitors of Pitting Corrosion in ASTM – A47 Low Carbon Steel in HCl Acid Environment. *Indonesia Journal of Chemistry*. 22 (1), 1–16.

[4] Ozoemena C. P, Godwin J. A and Ugwuoke, M. C. Corrosion inhibition and adsorption characteristics of Ethanolic extract of *brachystegia eurycoma* seed on the Corrosion of mild steel in 1m h2so4 acid solution. FUW Trends in Science and Technology Journal. 2021; 5 (2): 382–388.

[5] Samuel. N, Ogah S. P. I, Obike A, Igwe J. C, Ogbonna I. V (2015). Investigation of the Inhibitory Action of Brachystegia Eurycoma (Achi) Seed Extracts on the Corrosion of Mild Steel in 2M HCl by Method of Weight Loss. *International Journal Of Scientific Research And Education.* 3 (1), 3744-3753.

[6] M. Migahed, M. EL-Rabiei, H. Nady and E. Zaki. (2018). 1-(2-Aminoethyl)-1-dodecyl-2-undecyl-4,5-dihydro-1*H*-imidazol-1-ium chloride, 1-(2-Aminoethyl)-1-dodecyl-2-tridecyl-4,5-dihydro-1*H*-imidazol-1-ium chloride as Corrosion Inhibitors for Carbon Steel in Oil Wells Formation Water. *Journal of Molecular Structure*. 1159, 10–22.

[7] Ozoemena, C. P, Boekom, E. J and Inemesit, I. A. (2023). Synthesis, Characterization and Electrochemical Studies on the Corrosion Inhibition Properties of Schiff Bases for Mild Steel in 1 M HCl Solution. *Chemical Science International Journal.* 30 (2): 30 – 50.

[8] El-Lateef, HMA; Abu-Dief, AM; Mohamed, MAA. (2017). Corrosion inhibition of carbon steel pipelines by some novel Schiff base compounds during acidizing treatment of oil wells studied by electrochemical and quantum chemical methods. *Journal of Molecular Structure.* 1130: 522-542.

[9] Gergely, A., (2019). *Phenomenal and Theories in Corrosion Science: Methods of Prevention*, Nova Science Publishers Inc., USA.

[10] Onuchukwu, A. I., Oguzie, E. E. and Onuoha, G. N. (2004). Studies on the inhibitive action of methylene blue dye on aluminium corrosion in KOH solution. *Journal of Corrosion Science and Technology,* 1: 88–97.

[11] Haruna, A, Rumah, M. M, Sani, U and Ibrahim, A. K. (2020). Synthesis, Characterization and corrosion Inhibition Studies on Mn (II) and Co (II) Complexes Derived from 1-{(Z)-[(2-hydroxyphenyl) imino] methyl}naphthalen-2-ol in 1M HCl Solution. *International Journal of Biological, Physical and Chemical Studies.* (3) 1, 9-18.

[12] BoEkom, E. J, Essien K. E, Okafor P. C. (2016). Experimental and quantum studies: A new corrosion inhibitor for mild steel. *Elixir International Journal of corrosion and Dye.* 90, 37673-37678.

[13] Bardal, E. *Corrosion and Protection*. (2004). Springer-Verlag, London.

[14] Davis, J. R. *Corrosion: Understanding the Basics*, (2000). ASM International, USA.

[15] Ohtsuka, T., Nishikata, A., Sakari, M., and Fushimi, K. (2018). *Electrochemistry for Corrosion Fundamentals*. Springer, Singapore.

[16] Perez, N. *Electrochemistry and Corrosion Science*, 2nd Ed., (2016). Springer, Cham, Switzerland.

[17] Ugi B. U, Obeten M. E, Bassey M. V, Hitler L, Adalikwu S. A, Omaliko C. E, Nandi D. O, Uwah I. E. (2022). Adsorption and inhibition analysis of aconitine and tubocurarine alkaloids as eco-friendly inhibitors of pitting corrosion in ASTM – A47 Low Carbon Steel in HCl Acid Environment. *Indonesia Journal of Chemistry*. 22 (1), 1–16.

[18] Brezinski, M. M., Desai, B. (1997). Oil and Gas Pipeline Fundamentals. Google Patents.

[19] Walker, M. L. (1994). Method and composition for acidizing subterranean formations. Google Patents.

[20] Williams, D. A,. Holifield, P. K, Looney, J. R and McDougall, L. A. (1993). Inhibited acid system for acidizing wells. Google Patents.

[21] Yadav, M. Behera, D. (2012). Sharma, U. Inhibited acid system for acidizing wells. Arabian *Journal of Chemistry,* 3-12.

[22] Ituen, E. B., Akaranta, O. James, A. O. (2016). Elephant grass biomass extract as corrosion inhibitor for mild steel in acidic medium. *Journal of Chemical and Material Research*. 45–575.

[23] Ugi BU, Bassey V. M, Obeten M. E, Adalikwu S. A, Nandi D. O (2020). Secondary plant metabolites of natural product origin-*Strongylodon macrobotrys* as pitting corrosion inhibitors of steel around heavy salt deposits in Gabu, Nigeria, Journal of Material *Science and Chemical Engineering*. 8 (5), 38–60.

[24] EL Basiony N. M, Elgendy Amr, Nady H, Migahed M. A and Zaki E. G. (2019). Adsorption characteristics and inhibition effect of two Schiff base compounds on corrosion of mild steel in 0.5 M HCl solution. *RSC Adv.*, 9, 10473.

[25] Yang Xifeng, Feng Li and Weiwei Zhang (2019). 4-(Pyridin-4-yl) thiazol-2-amine as an efficient nontoxicinhibitor for mild steel in hydrochloric acidsolutions. *Royal Society of Chemistry;* (9): 10454–10464.

[26] Bashir, A. and Siraj, I. T. (2021). Synthesis, Characterization and Antimicrobial Studies of Schiff Base Derived from the Reaction of 2-Thiophenecarboxaldehyde and Ethylenediamine and its Metal (II) Complexes. *Chem search Journal of Chemical Society of Nigeria Kano Chapter*, 12 (1), 143 -148.

[27] Arora, M., Saravanan, J and Shivaji, S. B. (2013). Synthesis, characterization and antimicrobial activity of some Schiff bases of 2-amino-n-(p-acetamidophenyl carboxa, *International Journal of Pharmaceutical Science*., (8) 21, 1–12.

[28] Flores-Frias, E. A., Gonzalez-Hernandez, A,. Barba, V., Lopez-Sesenes, R, Landeros-Martinez L. L, Flores-De los Rios J. P. and Gonzalez-Rodriguez J. G. (2021). Experimental and theoretical evaluation of new 3,3´-methylenedianiline Schiff bases as corrosion inhibitors for carbon steel in sulfuric acid. *International Journal of Corrosion Science*, (10) 3, 1189–1212.

[29] Arulmurugan, S., Kavitha, H. P. and Venkatraman, B. R. (2010). Biological Activities of Schiff Base and its Complexes: A Review. *Rasayan Journal of Chemistry*, 3, 385-410.

[30] Mishra, M., Tiwari, K., Singh, A. K., & Singh, V. P. (2014). Synthesis, structural and corrosion inhibition studies on Mn (II), Cu (II) and Zn (II) complexes with a Schiff base derived from 2-hydroxypropiophenone. *Polyhedron*, (77), 57–65.

[31] Singh, A. Ahamad, I. Singh V and Quraishi, M. A. (2011). Corrosion Inhibition of Carbon Steel in HCl Solution by some Plant Extracts. International Journal of Corrosion Science, 15: 1087–1097.

[32] Gomathi V., Selvameena R., Subbalakshmi R., and Valarmathy, G (2013): Synthesis Characterization and antimicrobial studies Schiff Base Complexes of Mn (II), Co (II), Ni (II), Cu (II) and Zn (II) derived from 3-Amino Phenol And 2-Hydroxy-1-naphthaldehyde. *International Journal of Recent Scientific Research, 4* (1): 80-83.

[33] Kailas, K. H., Sheetal, J. P., Anita, P. P., and Apoorva, H. P. (2016). Four Synthesis Methods of Schiff Base Ligands and Preparation of Their Metal Complex With IR and Antimicrobial Investigation. *World Journal of Pharmacy and Pharmaceutical Sciences*. 5 (2), 1055–1063.

[34] Awe, F. E., Idris, S. O., Abdulwahab, M. and Oguzie, E. E. (2015) Theoretical and experimental inhibitive properties of mild steel in HCl by ethanolic extract of Boscia senegalensis. *Cogent Chemistry*. 1, 1–14.

[35] Eddy, N. O. and Odiongenyi, A. O. (2010). Corrosion Inhibition and Adsorption Properties of Ethanol Extract of IT heinsia crinata / IT on mild steel in H_2SO_4. *Pigment and Resin Technology.* 39 (5), 288–295.

[36] Yadav, S., Sharma, A., Choudhary, G., Monika and Sharma A. (2014). Inhibitive and adsorption properties of ethanolic extract of fruit of azadirachta indica on the corrosion of copper in HCL. *Int. J. Innov. Res. Sci. Eng. Tech.* 3, 16127–16136.

[37] Khaled, K. F. (2010). Corrosion control of copper in nitric acid solutions using some amino acids: A combined experimental and theoretical study. *Corrosion Science.* 52, 3225–3234.

[38] Roy P., and Sukul D. (2015). Corrosion inhibition of mild steel in acidic medium by polyacrylamide grafted Guar gum with various grafting percentage: effect of intramolecular synergism. *Corrosion Science.* 88, 246–253.

[39] Arukalam, I. O. (2014). Durability and synergistic effects of KI on the acid corrosion inhibition of mild steel by hydroxypropyl methylcellulose, Carbohydrate Polymer. *International Journal of Material Science.* 112, 291–299.

[40] Begum, A. S. Mallika, J. and Gayathri, P. (2010. Corrosion Inhibition Property of Some 1, 3, 4- Thiadiazolines on Mild Steel in Acidic Medium. *European Journal of Chemistry.* 58, 132–144.

[41] Abd El-Rehim, S. S., Magdy, A. Ibrahim, M. and Khaled, F. (1999). 4-Aminoantipyrine as an inhibitor of mild steel corrosion in HCl solution. Journal of Applied Electrochemistry. 29 (5), 593-599.

[42] Geary W. J. (1971). The use of conductivity measurements in organic solvents for characterization of coordination compounds. Coordination Chemistry Review. 7 (1), 81-122.

[43] Weaver G. W., Elsegood M. R., Tariq M., Amina M. (2016); synthesis and characterization of new Schiff base transition metal complexes derived from drug together with biological potential. Journal of Nuclear Medicine and Radiation Therapy 7 (6), 1-4.

[44] Boghaei, D. M., Askarizadeh, E., & Bezaatpour, A. (2008). Synthesis, characterization, spectroscopic and thermodynamic studies of charge transfer interaction of a new water-soluble cobalt (II) Schiff base complex with imidazole derivatives. *Spectrochim Acta A Mol Biomol Spectrosc.* 69 (2), 624–628.

[45] Shaker, A. M., Nassr, L. A. E and Adam, M. S. S. (2013). Hydrophilicity and acid hydrolysis of water-soluble antibacterial iron (II) Schiff base complexes in binary aqueous solvents. *Russian Journal of General Chemistry.* 83, 2460–2464.

[46] Aupers, J. H., Chohan, Z. H., Cox, P. J., Doidge-Harrison, S. M. S. V., Howie, A., Khan, A., Spencer, G. M., & Wardell, J. L. (1998). Syntheses and structures of diorgano (halo-orpseudohalo-) (1,3-dithiole-2-thione-4,5-dithiolato)-stannates (1-), [Q][R2SnX (dmit)] (Q=onium cation; X=halide orpseudohalide). *Polyhedron.* 17: (25–26).

[47] Chohan, Z. H., Wardell, J. L., Low, J. N., Meehan, P. R., & Ferguson, G. (1998). Tetraethylammoniumbromo (1,3-dithiol-2-one-4,5-dithiolato) diethylstannate (1-). *Acta Crystallographica Section C: Crystal Structure Communications.* 54 (10), 345-366.

[48] Selwood, P. W. (1956). *Magnetochemistry, Interscience*. chapter 2, p-78.

[49] Bertini, I. (2009). (Ed.). *Inorganic and Bio-Inorganic Chemistry-Vulume II (Vol. 6).*; EOLSS Publications.

[50] Nair, M. S., Arish, D., & Joseyphus, R. S. (2012). Synthesis, characterization, antifungal, antibacterial and DNA cleavage studies of some heterocyclic Schiff base metal complexes. Journal of Saudi Chemical Society. *16* (1), 83–88.

[51] Chohan, A. H., Che-Ani, A. I., Tahir, M. M., Abdullah, N. A. G., Tawil, N. M., and Kamaruzzaman, S. N. (2011). Housing and analysis of design defects: A post occupational evaluation of private housing in Malaysia. International Journal of Physical Sciences. 6 (2), 193–203.

[52] Alias, M., Kassum, H., and Shakir, C. (2014). Synthesis, physical characterization and biological evaluation of Schiff base M (II) complexes. Journal of the Association of Arab Universities for Basic and Applied Sciences. *15* (1), 1002-1016.

[53] Ferraro, J. R. (1971). Metal Halide Vibrations. In *Low-Frequency Vibrations of Inorganic and Coordination Compounds.* Springer, Boston, MA. 111-189.

[54] Nakamoto K. (2009). *Infrared and Raman spectra of inorganic and coordination compounds, part B: applications in coordination, organometallic, and bioinorganic chemistry.* John Wiley & Sons.

[55] Tandon, J. P., Crowe, A. J., & Road, F. (1986). Synthesis and Structural Studies of Tin (II) Complexes of Semicarbazones and Thiosemicarbazones. *Polyhedron, 5* (3), 739–742.

[56] Eddy, N. O., Awe, F. E., Gimba, N. O. and Ebenso, E. E. (2011). Inhibitive effect of Prosopis cineraria on mild steel in acidic media*. International Journal of Electrochemical Science*. 6, 920–931.

[57] Okoronkwo, A. E., Olusegun, S. J. and Olaniran, O. (2015). Acid extract of Gliricidia sepium leaves as green corrosion inhibitor for mild steel in HCl solutions. *African corrosion Journal.* 1: 30–35.

[58] Ugi B. U, Obeten M. E. Bassey V. M. Boekom E. J, Omaliko E. C, Ugi F. B, Uwah I. E. (2021). Quantum and electrochemical studies of corrosion inhibition impact on industrial structural steel (E410) by expired amiloride drug in 0.5 M solutions of HCl, H_2SO_4 and $NaHCO_3$. *Moroccan Journal of Chemistry.* 9 (4), 677–696.

[59] Ejikeme, P. M, Umana, S. G, Menkiti, M. C. and Onukwuli, O. D. (2015). Inhibition of mild steel and aluminum corrosion in 1M H_2SO_4 by leaves extract of African breadfruit. *International Journal of Material Science.* 5 (1), 14-23.

[60] Aouniti, H., Elmsellem, A., Tighadouini, S., Elazzouzi, M., Radi, S., Chetouani, A., Hammouti, B., and Zarrouk, A. (2016). Schiff's base derived from 2-acetyl thiophene as corrosion inhibitor of steel in acidic medium. *Journal of Taibah University for Science*. 10 (5), 774-785.

[61] Charles, A., Sivaraj, K., and Thanikaikarasan, S. (2020): "Synthesis, characterization and corrosion studies of Schiff bases derived from pyrrole- 2-carbaldehyde*", Materials Today Proceedings*. 4, 157–183.

[62] El-Tabesh, R. N., Abdel-Gaber, A. M., Hammud, H. H., & Al-Oweini, R. (2020). Correction to: Effect of Mixed-Ligands Copper Complex on the Corrosion Inhibition of Carbon Steel in Sulfuric Acid Solution. *Journal of Bio- and Tribo-Corrosion*, 6 (2), 467-488.

[63] Gupta, N. K., Verma, C., Quraishi, M. A., and Mukhrajee, A. K. (2016): "Schiff's Base Derived from L-lysine and Aromatic Aldehydes as Green Corrosion Inhibitors for Mild Steel: Experimental and theoretical studies", *Journal of Molecular Liquids*. 15, 47–57.

[64] Anupama, K. K. (2015). Corrosion inhibition study of medicinal plant extracts and some of their components for mild steel in acid media. M. Sc Thesis, Department of Chemistry, University of Calicut. 6, 997-1015.

[65] Guo, L; Safi, ZS; Kaya, S; Shi, W; Tuzun, B; Altunay, N; Kaya, C (2018). Anticorrosive effects of some thiophene derivatives against the corrosion of iron: a computational study. *Frontier Chemistry Journal,* 6 (5): 15-26.

[66] Solomon, M. M and Umoren, S. A. (2015). Electrochemical and gravimetric measurements of inhibition of aluminum corrosion by poly (methacrylic acid) in H_2SO_4 solution and synergistic effect of iodide ions. *Journal of Adhesion Science Technology*. 76: 104–116.

[67] Ituen, E. B., Onyewuchi, A. and Abosede, J. (2017). Evaluation of Performance of Corrosion Inhibitors Using Adsorption Isotherm Models: An Overview. Chemical Science International Journal, 18 (1), 1-34.

[68] Oguzie, E. E. (2007). Corrosion inhibition of aluminum in acidic and alkaline media by Sansevieria trifasciata extract. *Corrosion Science Journal*. 49, 1527–1539.

[69] Ebenso, E. E. (2004). Effect of halide ions on the corrosion inhibition of mild steel in H_2SO_4 using methyl red. *Bulletin of Electrochemisry*. 19 (5): 209-216.

[70] Erdogan, S; Zaki, SS; Kaya, S; Isin, DÖ; Guo, L; Kaya, C (2017). A computational study on corrosion inhibition performances of novel quinoline derivatives against the corrosion of iron. *Journal of Molecular Structure,* 1134: 751-761.

[71] Loto, C. A. (2011). Inhibition effect of tea (Camellia Sinensis) extract on the corrosion of mild steel in dilute sulphuric acid. *Journal of Materials and Environmental Science.* 2, 335–344.

[72] Ikeuba, A. I., Zhang, B., Wamg, J. and Okafor, P. C. "SVET and SIET (2018). Study of Galvanic corrosion of Al/$MgZn_2$ in aqueous solutions at different PH". *Journal of the Electrochemical Society.* 165, 1043-1049.

[73] Atkins, P. and Julio, D., (2010). *Atkins' Physical Chemistry. 9th ed.* Oxford University Press, Great Clarendon Street, Oxford, Ox2 6DP. United State, 685.

[74] Okafor, P. C., Ebiekpe, V. E., Azike, C. F., Egbung, G. E., Brisibe, E. A., and Ebenso E. E.. Inhibitory Action of Artemisia annua Extracts and Artemisinin on the Corrosion of Mild Steel in H_2SO_4 Solution. International Journal of Corrosion. 2012; 20 (6), 8–19.

[75] Obot, I. B, Obi-Egbedi, N. O. and Umoren, S. A., (2012). Adsorption Characteristics and Corrosion Inhibitive Properties of Clotrimazole for Aluminium Corrosion in Hydrochloric Acid. *International Journal of Electrochemical Science*. 4, 863–877.

[76] Ekuma, F. K., Odoemelam, S. A., Ekanem, U. I. and Okoyeagu, A. (2018). Synthesized Schiff bases from linoleic and benheric acids as inhibitor of mild steel corrosion in HCl medium. Research Journal of Chemical Sciences. 8 (9), 12–25.